Chapter 6

Offset, another dimension

Earlier chapters have assumed that the shot and the geophone are located in the same place. The reality is that there is often as much as a 3-km horizontal separation between them. The 3-km offset is comparable to the depth of many petroleum reservoirs.

Offset is another *dimension* in the analysis of data. At the time of writing, this dimension is often represented in field operations by about 48 channels. No one seems to believe, however, that 48 channels is enough. Recording systems with as many as 1024 channels are coming into use.

The offset dimension adds three important aspects to reflection seismology. First, it enables us to routinely measure the velocity of seismic waves in rocks. This velocity has been assumed to be known in the previous chapters of this book. Second, it gives us data redundancy: it gives independent measurements of quantities that should be the same. Superposition of the measurements (stacking) offers the potential for signal enhancement by destructive interference of noise. Third (a disadvantage), since the offset is nonzero, procedures for migration take on another element of complexity. By the end of this chapter we will be trying to deal with three confusing subjects at the same time—dip, offset, and lateral velocity variation.

Theoretically it seems that offset should offer us the possibility of identifying rocks by observing the reflection coefficient as a function of angle, both for P waves and for P-to-S converted waves. The reality seems to be that neither measurement can be made reliably, if at all. See elswhere in this book a fuller discussion of converted waves, an interesting subject for research, with a large potential for practical rewards. See also Ostrander [1984] and Tatham and Stoffa [1976]. The reasons for the difficulty in measurement, and the resolution of the difficulty, are, however, not the goal of this book. This goal is instead to enable us to deal effectively with that which is routinely observable.

6.0.1 Stacking diagrams

First, define the midpoint y between the shot and geophone, and define h to be half the horizontal offset between the shot and geophone:

$$y = \frac{g + s}{2} \tag{6.1}$$

$$h = \frac{g - s}{2} \tag{6.2}$$

The reason for using *half* the offset in the equations is to simplify and symmetrize many later equations. Offset is defined with $g - s$ rather than with $s - g$ so that positive offset means waves moving in the positive x direction. In the marine case, this means the ship is presumed to sail negatively along the x-axis. In reality the ship may go either way, and shot points may either increase or decrease as the survey proceeds. In some situations you can clarify matters by setting the field observer's shot-point numbers to negative values.

Data is defined experimentally in the space of $(s,\ g)$. Equations (1.1) and (1.2) represent a change of coordinates to the space of $(y,\ h)$. Midpoint-offset coordinates are especially useful for interpretation and data processing. Since the data is also a function of the travel time t, the full dataset lies in a volume. Because it is so difficult to make a satisfactory display of such a volume, what is customarily done is to display slices. The names of slices vary slightly from one company to the next. The following names seem to be well known and clearly understood:

$(y,\ h = 0,\ t)$	zero-offset section
$(y,\ h = h_{\rm min},\ t)$	near-trace section
$(y,\ h = {\rm const},\ t)$	constant-offset section
$(y,\ h = h_{\rm max},\ t)$	far-trace section
$(y = {\rm const},\ h,\ t)$	common-midpoint gather
$(s = {\rm const},\ g,\ t)$	field profile (or common-shot gather)
$(s,\ g = {\rm const},\ t)$	common-geophone gather
$(s,\ g,\ t = {\rm const})$	time slice
$(h,\ y,\ t = {\rm const})$	time slice

A diagram of slice names is in Figure 1.1. Figure 1.2 shows three slices from the data volume. The first mode of display is "engineering drawing mode." The second mode of display is on the faces of a cube. But notice that although the data is displayed on the surface of a cube, the slices themselves are taken from the interior of the cube. The intersections of slices across one another are shown by dark lines.

A common-depth-point (CDP) gather is defined by the industry and by common usage to be the same thing as a common-midpoint (CMP) gather. But in this book a distinction will be made. A CDP gather is a CMP gather with its time axis stretched according to some velocity model, say,

$$(y = {\rm const},\ h,\ \sqrt{t^2 - 4h^2/v^2} \quad \text{common-depth-point gather}$$

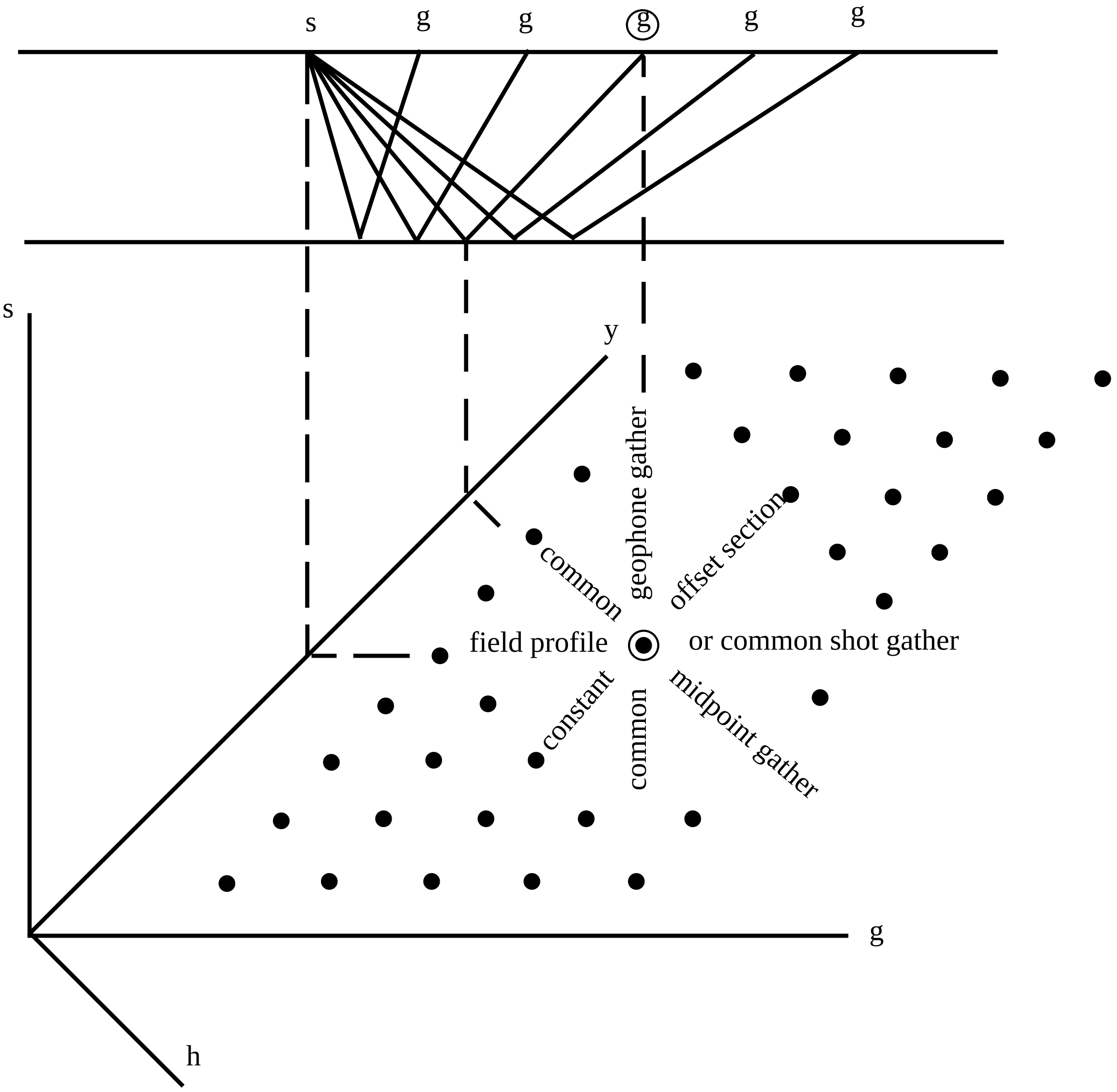

Figure 6.1: Top shows field recording of marine seismograms from a shot at location s to geophones at locations labeled g. There is a horizontal reflecting layer to aid interpretation. The lower diagram is called a stacking diagram. (It is *not* a perspective drawing). Each dot in this plane depicts a possible seismogram. Think of time running out from the plane. The center geophone above (circled) records the seismogram (circled) that may be found in various geophysical displays. Labels in the diagram below give common names for the displays. ofs-sg [NR]

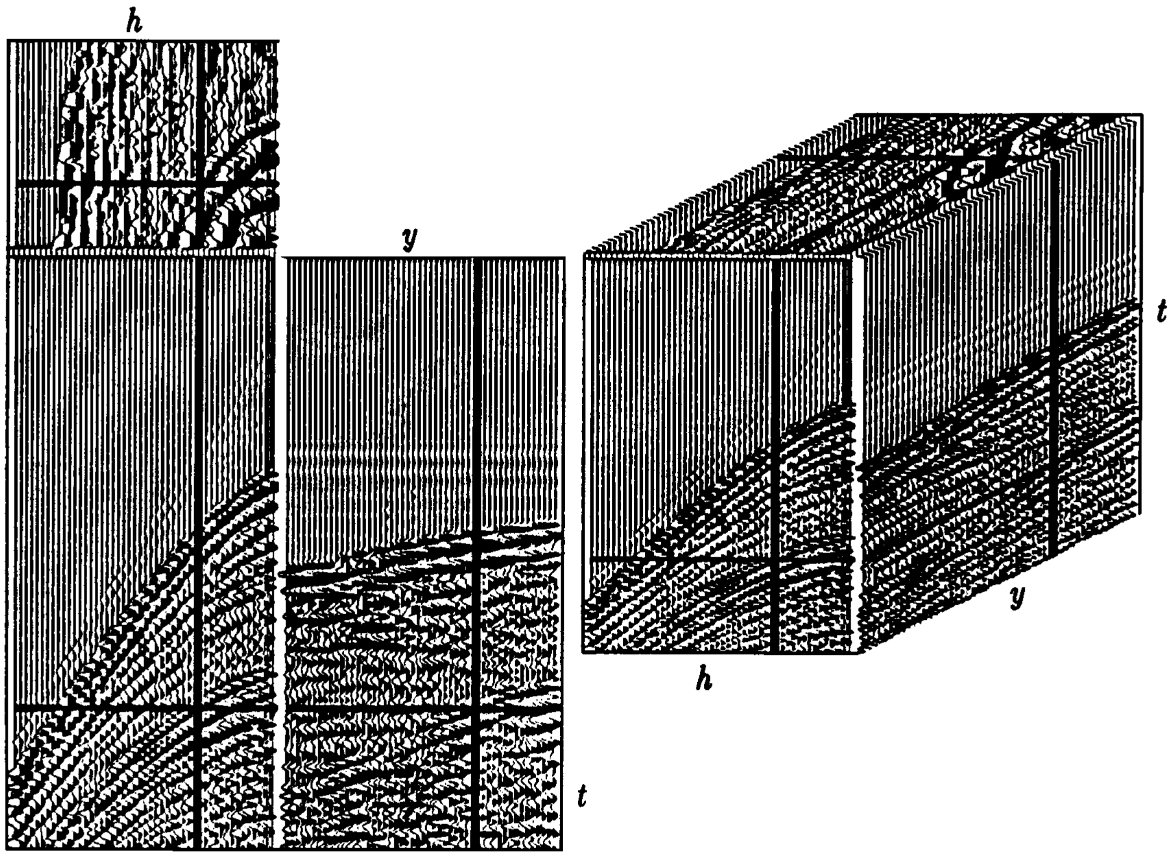

Figure 6.2: Slices from a cube of data from the Grand Banks. Left is "engineering drawing" mode. At the right slices from within the cube are shown as faces on the cube. (Data from Amoco. Display via Rick Ottolini's movie program). ofs-rick [NR]

This offset-dependent stretching makes the time axis of the gather become more like a *depth* axis, thus providing the D in CDP. The stretching is called *normal moveout correction* (NMO). Notice that as the velocity goes to infinity, the amount of stretching goes to zero.

In industrial practice the data is not routinely displayed as a function of offset. Instead, each CDP gather is summed over offset. The resulting sum is a single trace. Such a trace can be constructed at each midpoint. The collection of such traces, a function of midpoint and time, is called a CDP stack. Roughly speaking, a CDP stack is like a zero-offset section, but it has a less noisy appearance.

The construction of a CDP stack requires that a numerical choice be made for the moveout-correction velocity. This choice is called the *stacking velocity* . The stacking velocity may be simply someone's guess of the earth's velocity. Or the guess may be improved by stacking with some trial velocities to see which gives the strongest and least noisy CDP stack.

Figure 1.3 shows typical land and marine profiles (common-shot gathers). The

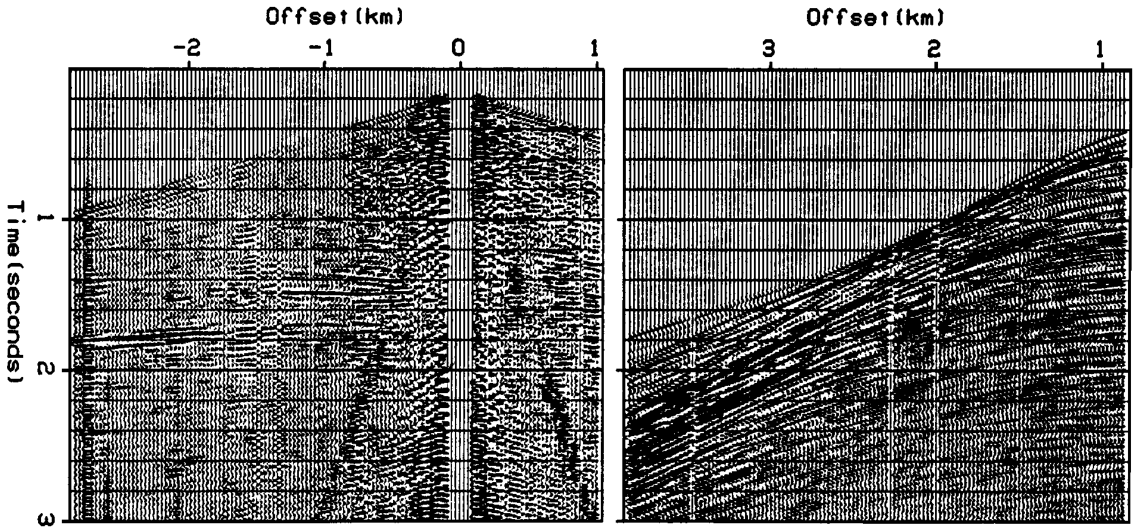

Figure 6.3: Field profiles. Left is a land profile from West Texas. Right is a marine profile off the Aleutian Islands. (Western Geophysical). ofs-profiles [NR]

land data has geophones on both sides of the source. The arrangement shown is called an *uneven split spread* . The energy source was a vibrator. The marine data happens to nicely illustrate two or three head waves. The marine energy source was an air gun. These field profiles were each recorded with about 120 geophones.

6.0.2 What is "poor quality" data?

Vast regions of the world have good petroleum potential but are hard to explore because of the difficulty of obtaining good quality reflection seismic data. The reasons are often unknown. What is "poor quality" data? From an experimental view, almost all seismic data is good in the sense that it is repeatable. The real problem is that the data makes no sense.

Take as an earth model a random arrangement of point reflectors. Its migrated zero-offset section should look random too. Given the repeatability that is experienced in data collection, data with a random appearance implies a random jumble of reflectors. With only zero-offset data little else can be deduced. But with the full range of offsets at our disposal, a more thoughtful analysis can be tried. This chapter provides some of the required techniques.

An interesting model of the earth is a random jumble of point scatterers in a constant-velocity medium. The data would be a random function of time and a random function of the horizontal location of the shot-geophone midpoint. But after suitable processing, for each midpoint, the data should be a perfectly hyperbolic function of shot-geophone offset. This would determine the earth velocity exactly, even if the random scatterers were distributed in three dimensions, and the survey were only along a surface line.

This particular model could fail to explain the "poor quality" data. In that case other models could be tried. The effects of random velocity variations in the near surface or the effects of multiple reflections could be analyzed. Noise in seismology can usually be regarded as a failure of analysis rather than as something polluting the data. It is the offset dimension that gives us the redundancy we need to try to figure out what is really happening.

6.0.3 Texture of horizontal bedding, marine data

Gravity is a strong force for the stratification of rocks, and in many places in the world rocks are laid down in horizontal beds. Yet even in the most ideal environment the bedding is not mirror smooth; it has some *texture.* We begin the study of offset with synthetic data that mimics the most ideal environment. Such an environment is almost certainly marine, where sedimentary deposition can be slow and uniform. The wave velocity will be taken to be constant, and all rays will reflect as from horizontally lying mirrors. Mathematically, *texture* is introduced by allowing the reflection coefficients of the beds to be laterally variable. The lateral variation is presumed to be a random function, though not necessarily with a white spectrum. Let us examine the appearance of the resulting field data.

Randomness is introduced into the earth with a random function of midpoint y and depth z. This randomness is impressed on some geological "layer cake" function of depth z. For every point in (y, z)-space, a hyperbola of the appropriate random amplitude must be superposed in the space of offset h and travel time t.

What does the final data space look like? This question has little meaning until we decide how the three-dimensional data volume will be presented to the eye. Let us view the data much as it is recorded in the field. For each shot point we see a frame in which the vertical axis is the travel time and the horizontal axis is the distance from the ship down the towed hydrophone cable. The next shot point gives us another frame. Repetition gives us the accompanying program that produces a cube of data, hence a move. This cube is synthetic data for the ideal marine environment. And what does the movie show?

```
subroutine synmarine ( data, nt,nh,ny, nz)
integer                       nt,nh,ny, nz,    it,ih,iy,is,iz, ns, iseed
          real         data( nt,nh,ny),       layer, rand01
temporary real                          refl(nz,ny), depth(nz)
iseed= 1992;    ns = ny
do iz= 1, nz {                                  # 0 < rand01() < 1
        depth( iz) =  nt * rand01(iseed)        # Reflector depth
        layer      =  2. * rand01(iseed) - 1.   # Reflector strength
        do iy= 1, ny {                          # Impose texture on layer
                refl(iz,iy) = layer * (1. + rand01(iseed))
                }
        }
call null(             data, nt*nh*ny)          # erase data space
do is= 1, ns    {                               # shots
do ih= 1, nh    {                               # down cable h = (g-s)/2
do iz= 1, nz    {                               # Add hyperbola for each layer
        iy = (ns-is)+(ih-1)                     # y = midpoint
        iy = 1 + (iy-ny*(iy/ny))                # periodic with midpoint
        it = 1 + sqrt( depth(iz)**2 + 25.*(ih-1)**2 )
        if( it <= nt)
                data(it,ih,is) = data(it,ih,is) + refl(iz,iy)
        }}}
return; end
```

A single frame shows hyperbolas with imposed texture. The movie shows the texture moving along each hyperbola to increasing offsets. (I find that no sequence of still pictures can give the impression that the movie gives). Really the ship is moving; the texture of the earth is remaining stationary under it. This is truly what most marine data looks like, and the subroutine `synmarine()` simulates it.

Comparing the simulated data to real marine-data movies, I am impressed by the large amount of random lateral variation required in the simulated data to achieve resemblance to field data. The randomness seems too great to represent lithologic variation. Apparently it is the result of something not modeled. Perhaps it results from our incomplete understanding of the mechanism of reflection from the quasi-random earth. Or perhaps it is an effect of the partial focusing of waves sometime after they reflect from minor topographic irregularities.

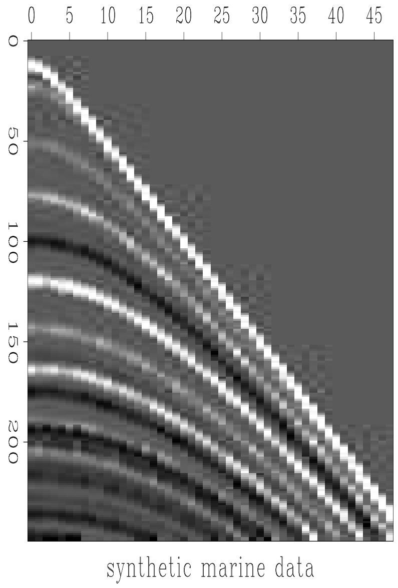

Figure 6.4: A frame from the synthetic marine data subroutine `synmarine()`. Press button for movie. ofs-synmarine [ER]

6.0.4 Texture of land data: near-surface problems

Reflection seismic data recorded on land frequently displays randomness because of the irregularity of the soil layer. Often it is so disruptive that the seismic energy sources are deeply buried (at much cost). The geophones are too many for burial. For most land reflection data, the texture caused by these near-surface irregularities exceeds the texture resulting from the reflecting layers.

To clarify our thinking, an ideal mathematical model will be proposed. Let the reflecting layers be flat with no texture. Let the geophones suffer random time delays of several time points. Time delays of this type are called *statics.* Let the shots have random strengths. For this movie, let the data frames be *common-midpoint gathers,* that is, let each frame show data in (h, t)-space at a fixed midpoint y. Successive frames will show successive midpoints. The study of Figure 1.1 should convince you that the travel-time irregularities associated with the geophones should move leftward, while the amplitude irregularities associated with the shots should move rightward. In real life, both amplitude and time anomalies are associated with both shots and geophones.

EXERCISES:

1 Note that Figure 1.1 is drawn for a shot interval Δs equal to half the geophone interval Δg. Redraw Figure 1.1 for $\Delta s = \Delta g$. Common-midpoint gathers now come in two types. Suggest two possible definitions for "near-offset section."

2 Modify the program of Figure 1.5 to produce a movie of synthetic *midpoint* gathers with random shot amplitudes and random geophone time delays. Observing this movie you will note the perceptual problem of being able to see the leftward

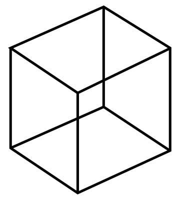

Figure 6.5: ofs-cube [NR]

motion along with the rightward motion. Try to adjust anomaly strengths so that both left-moving and right-moving patterns are visible. Your mind will often see only one, blocking out the other, similar to the way you perceive a 3-D cube, from a 2-D projection of its edges.

3 Define recursive dip filters to pass and reject the various textures of shot, geophone, and midpoint.

6.1 ABSORPTION AND A LITTLE FOCUSING

Sometimes the earth strata lie horizontally with little irregularity. There we may hope to ignore the effects of migration. Seismic rays should fit a simple model with large reflection angles occurring at wide offsets. Such data should be ideal for the measurement of reflection coefficient as a function of angle, or for the measurement of the earth acoustic absorptivity $1/Q$. In his doctoral dissertation, Einar Kjartansson reported such a study. The results were so instructive that the study will be thoroughly reviewed here. I don't know to what extent the Grand Isle gas field (Pan [1983]) typifies the rest of the earth, but it is an excellent place to begin learning about the meaning of shot-geophone offset.

6.1.1 The grand isle gas field: a classic bright spot

The dataset Kjartansson studied was a seismic line across the Grand Isle gas field, off the shore of Louisiana, and was supplied by the Gulf Oil Company. The data contain several classic "bright spots" (strong reflections) on some rather flat undisturbed bedding. Of interest are the lateral variations in amplitude on reflections at a time depth of about 2.3 seconds. (See Figure 1.8. It is widely believed that such bright spots arise from shallow gas-bearing sands.

Theory predicts that reflection coefficient should be a function of angle. For an anomalous physical situation like gas-saturated sands, the function should be distinctive. Evidence should be found on common-midpoint gathers like those shown in Figure 1.6. Looking at any one of these gathers you will note that the reflection strength versus offset seems to be a smooth, sensibly behaved function, apparently quite measurable. Using layered media theory, however, it was determined that only

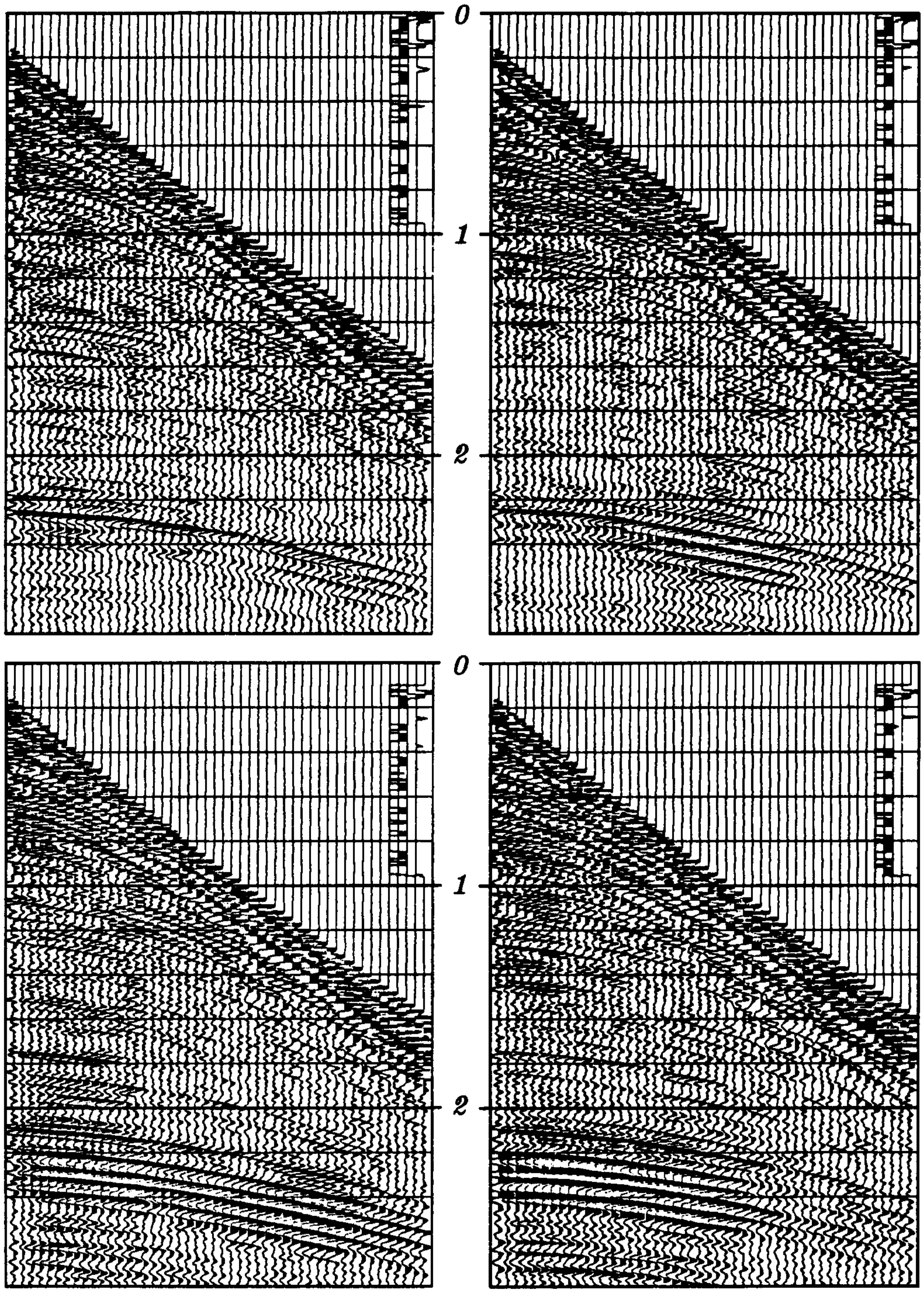

Figure 6.6: Top left is shot point 210; top right is shot point 220. No processing has been applied to the data except for a display gain proportional to time. Bottom shows shot points 305 and 315. (Kjartansson, Gulf) ofs-kjcmg [NR]

the most improbably bizarre medium could exhibit such strong variation of reflection coefficient with angle, particularly at small angles of incidence. (The reflection angle of the energy arriving at wide offset at time 2.5 seconds is not a large angle. Assuming constant velocity, $\arccos(2.3/2.6) = 28^\circ$). Compounding the puzzle, each common-midpoint gather shows a *different* smooth, sensibly behaved, measurable function. Furthermore, these midpoints are near one another, ten shot points spanning a horizontal distance of 820 feet.

6.1.2 Kjartansson's model for lateral variation in amplitude

The Grand Isle data is incomprehensible in terms of the model based on layered media theory. Kjartansson proposed an alternative model. Figure 1.7 illustrates a geometry in which rays travel in straight lines from any source to a flat horizontal reflector, and thence to the receivers. The only complications are "pods" of some material that is presumed to disturb seismic rays in some anomalous way. Initially you may imagine that the pods absorb wave energy. (In the end it will be unclear whether the disturbance results from energy focusing or absorbing).

Pod A is near the surface. The seismic survey is affected by it twice—once when the pod is traversed by the shot and once when it is traversed by the geophone. Pod C is near the reflector and encompasses a small area of it. Pod C is seen at all offsets h but only at one midpoint, y_0. The raypath depicted on the top of Figure 1.7 is one that is affected by all pods. It is at midpoint y_0 and at the widest offset h_{max}. Find the raypath on the lower diagram in Figure 1.7.

Pod B is part way between A and C. The slope of affected points in the (y, h)-plane is part way between the slope of A and the slope of C.

Figure 1.8 shows a common-offset section across the gas field. The offset shown is the fifth trace from the near offset, 1070 feet from the shot point. Don't be tricked into thinking the water was deep. The first break at about .33 seconds is wide-angle propagation.

The power in each seismogram was computed in the interval from 1.5 to 3 seconds. The logarithm of the power is plotted in Figure 1.9a as a function of midpoint and offset. Notice streaks of energy slicing across the (y, h)-plane at about a 45° angle. The strongest streak crosses at exactly 45° through the near offset at shot point 170. This is a missing shot, as is clearly visible in Figure 1.8. Next, think about the gas sand described as pod C in the model. Any gas-sand effect in the data should show up as a streak across all offsets at the midpoint of the gas sand—that is, horizontally across the page. I don't see such streaks in Figure 1.9a. Careful study of the figure shows that the rest of the many clearly visible streaks cut the plane at an angle noticeably *less* than $\pm 45^\circ$. The explanation for the angle of the streaks in the figure is that they are like pod B. They are part way between the surface and the reflector. The angle determines the depth. Being closer to 45° than to 0°, the pods are closer to the surface than to the reflector.

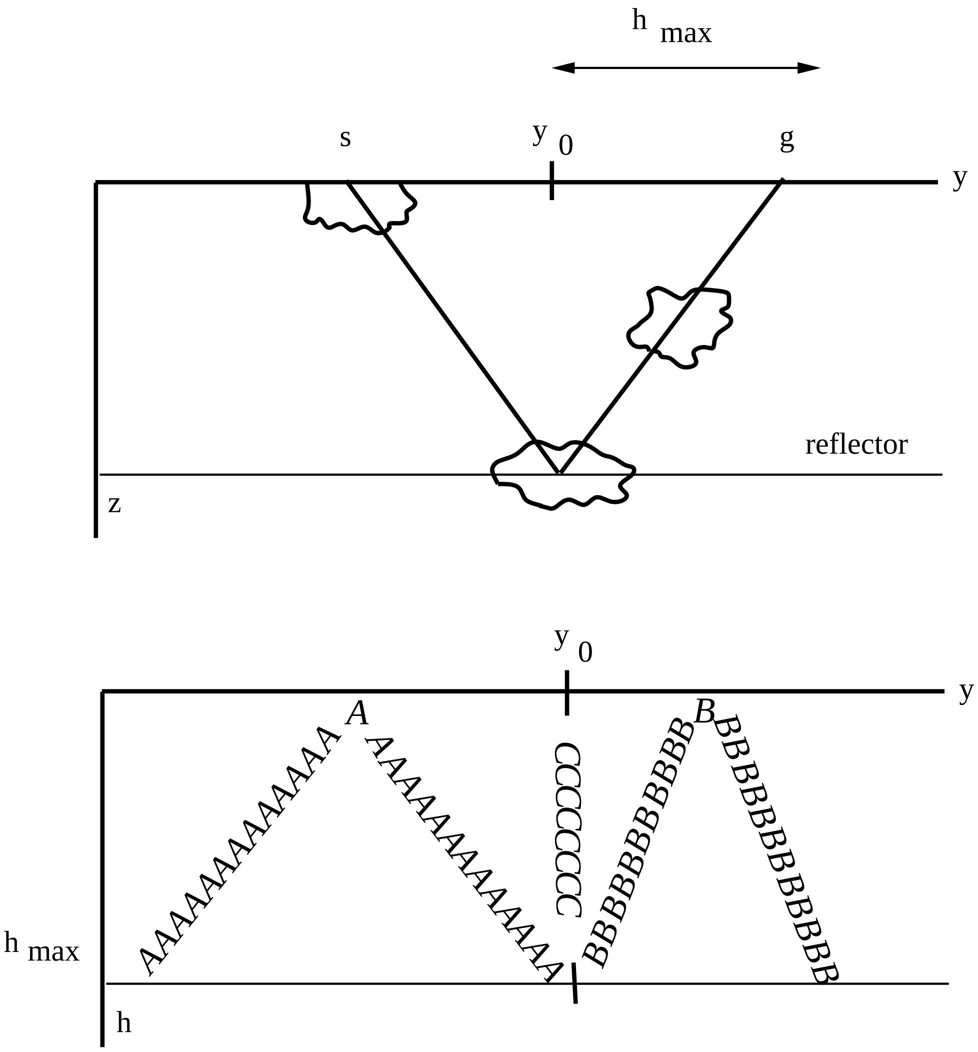

Figure 6.7: Kjartansson's model. The model on the top produces the disturbed data space sketched below it. Anomalous material in pods A, B, and C may be detected by its effect on reflections from a deeper layer. ofs-kjidea [NR]

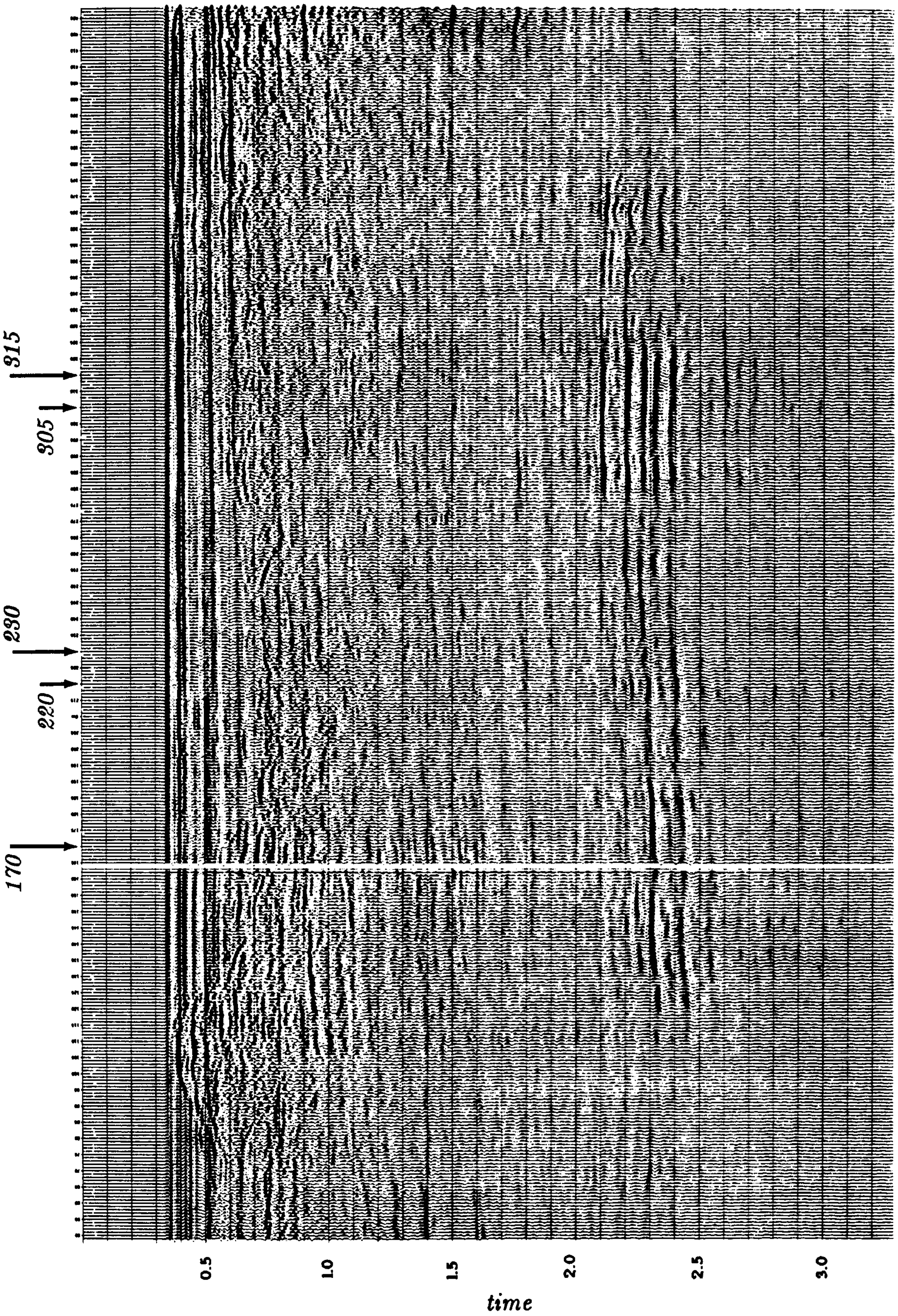

Figure 6.8: A constant-offset section across the Grand Isle gas field. The offset shown is the fifth from the near trace. (Kjartansson, Gulf) ofs-kjcos [NR]

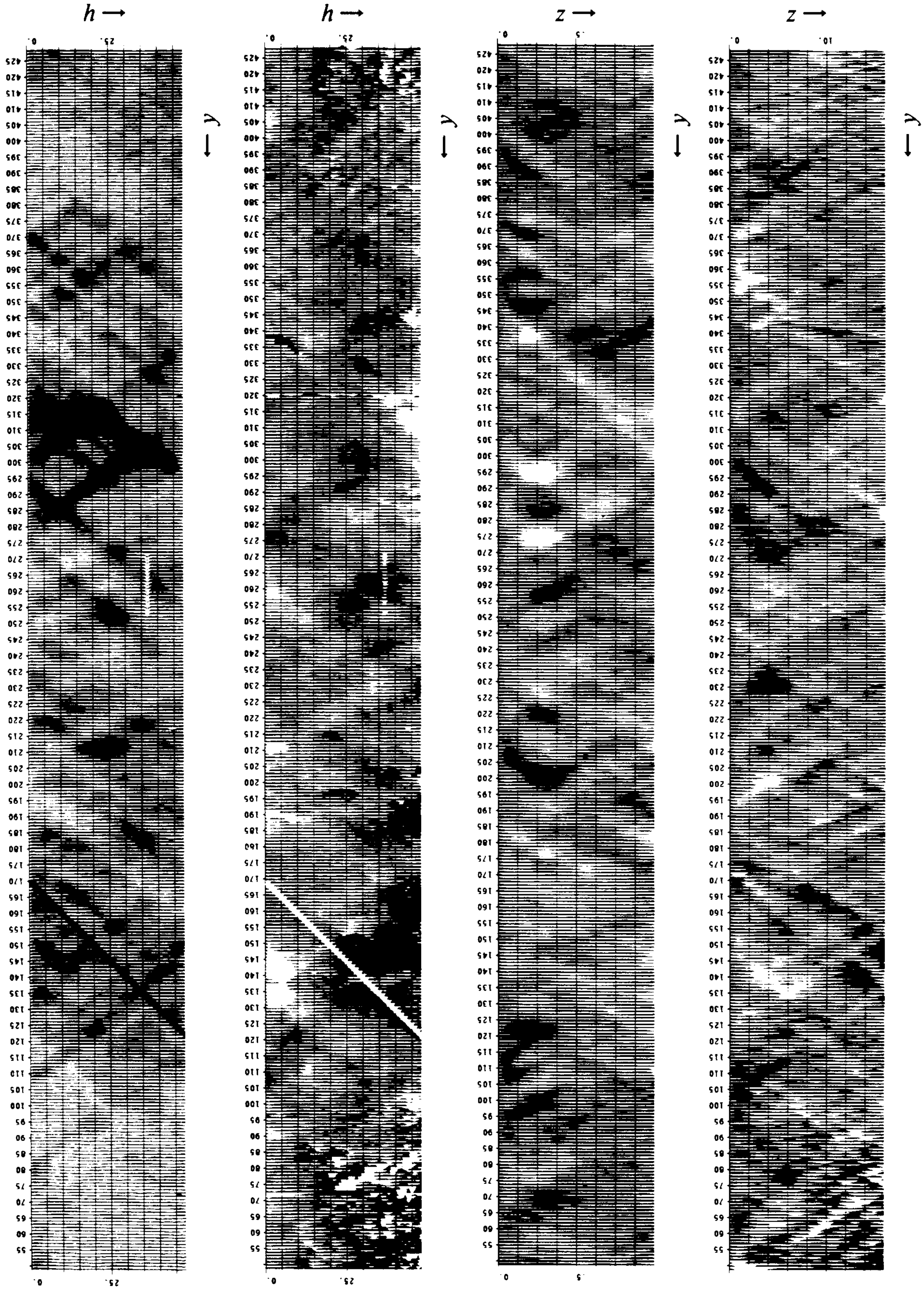

Figure 6.9: (a) amplitude (h,y), (b) timing (h,y) (c) amplitude (z,y), (d) timing (d,y) ofs-kja [NR]

Figure 1.9b shows timing information in the same form that Figure 1.9a shows amplitude. A CDP stack was computed, and each field seismogram was compared to it. A residual time shift for each trace was determined and plotted in Figure 1.9b. The timing residuals on one of the common-midpoint gathers is shown in Figure 1.10.

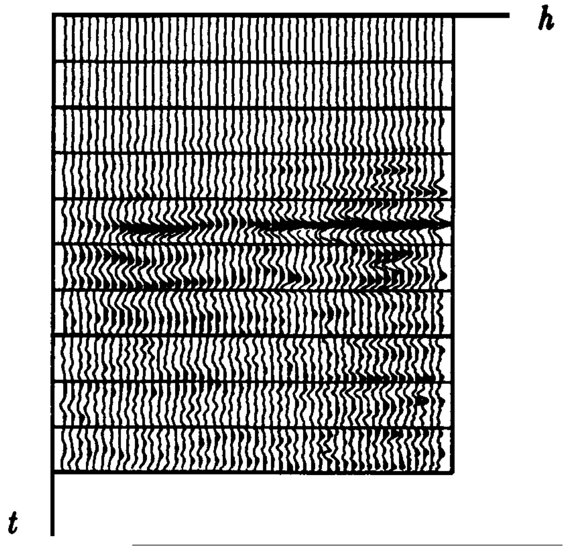

Figure 6.10: Midpoint gather 220 (same as timing of (h,y) in Figure 1.9b) after moveout. Shown is a one-second window centered at 2.3 seconds, time shifted according to an NMO for an event at 2.3 seconds, using a velocity of 7000 feet/sec. (Kjartansson) ofs-kjmid [NR]

The results resemble the amplitudes, except that the results become noisy when the amplitude is low or where a "leg jump" has confounded the measurement. Figure 1.9b clearly shows that the disturbing influence on timing occurs at the same depth as that which disturbs amplitudes.

The process of *inverse slant stack* , to be described in Section 5.2 enables us to determine the depth distribution of the pods. This distribution is displayed in figures 1.9c and 1.9d.

6.1.3 Rotten alligators

The sediments carried by the Mississippi River are dropped at the delta. There are sand bars, point bars, old river bows now silted in, a crow's foot of sandy distributary channels, and between channels, swampy flood plains are filled with decaying organic material. The landscape is clearly laterally variable, and eventually it will all sink of its own weight, aided by growth faults and the weight of later sedimentation. After it is buried and out of sight the lateral variations will remain as pods that will be observable by the seismologists of the future. These seismologists may see something like Figure 1.11. Figure 1.11 shows a *three-dimensional* seismic survey, that is, the ship sails many parallel lines about 70 meters apart. The top plane, a slice at constant time, shows buried river meanders. The data shown in Figure 1.11 is described more fully by its donors, Dahm and Graebner [1982].

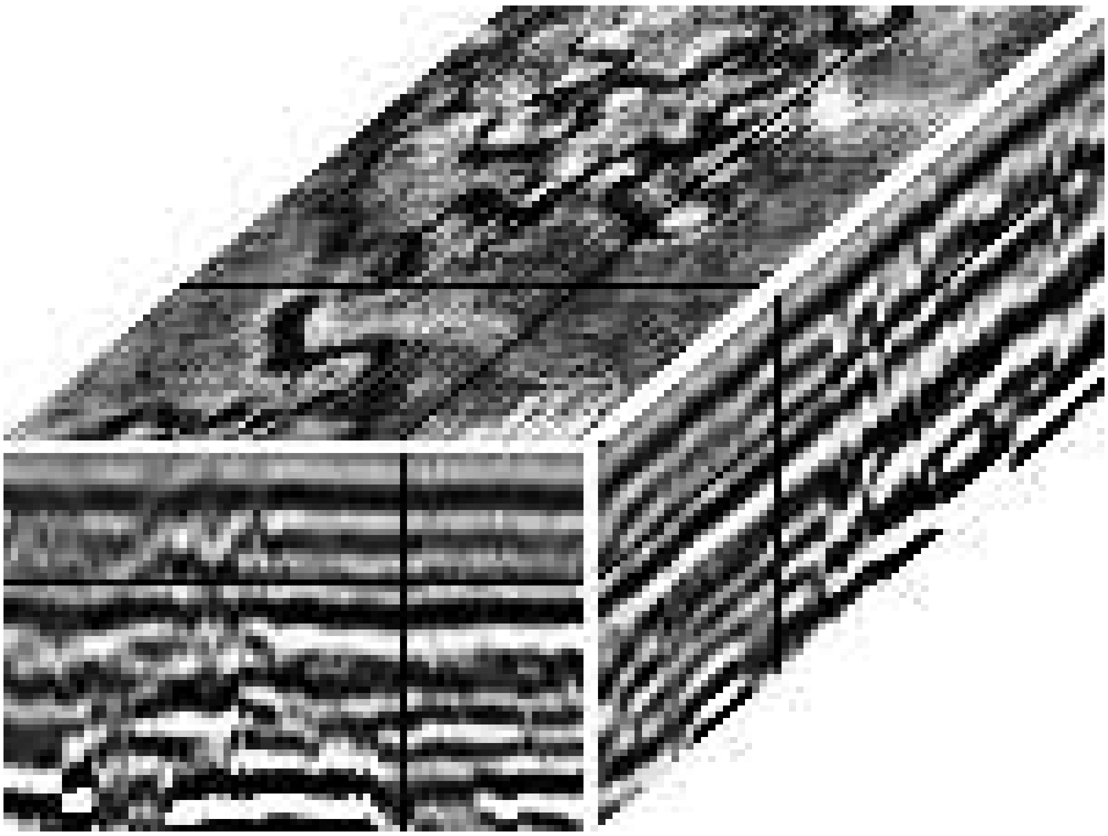

Figure 6.11: Three-dimensional seismic data (Geophysical Services Inc.) from the Gulf of Thailand. Data planes from within the cube are displayed on the faces of the cube. The top plane shows ancient river meanders now submerged. ofs-meander [ER]

6.1.4 Focusing or absorption?

Highly absorptive rocks usually have low velocity. Behind a low velocity pod, waves should be weakened by absorption. They should also be strengthened by focusing. Which effect dominates? How does the phenomenon depend on spatial wavelength? A full reconstruction of the physical model remains to be done. Maybe you can figure it out knowing that black on Figure 1.9c denotes low amplitude or high absorption, and black on Figure 1.9d denotes low velocities.

EXERCISES:

1 Consider waves converted from pressure P waves to shear S waves. Assume an S-wave speed of about half the P-wave speed. What would Figure 1.7 look like for these waves?

6.2 INTRODUCTION TO DIP

The study of seismic travel-time dependence upon source-receiver offset begins by calculating the travel times for rays in some ideal environments.

6.2.1 Sections and gathers for planar reflectors

The simplest environment for reflection data is a single horizontal reflection interface, which is shown in Figure 1.12. As expected, the zero-offset section mimics the earth

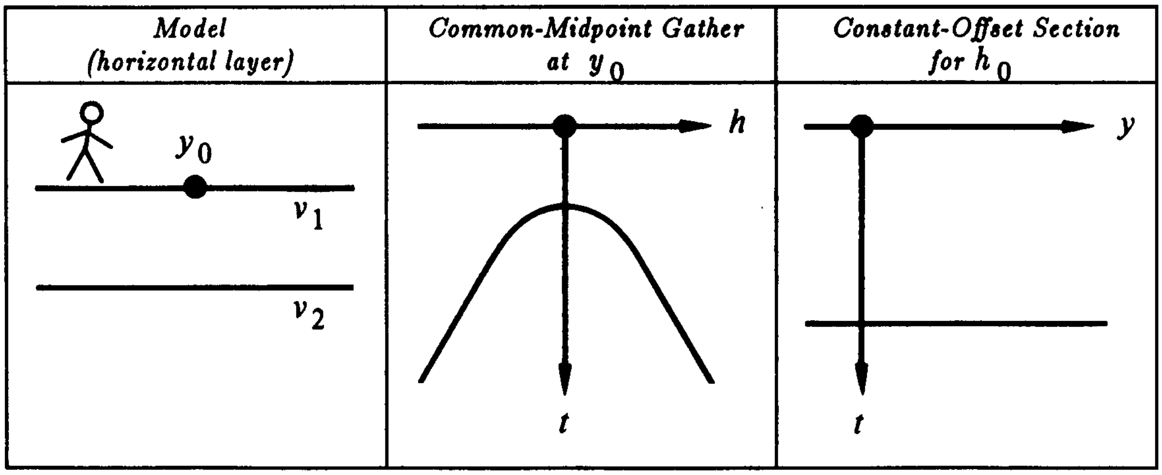

Figure 6.12: Simplest earth model. $\boxed{\text{ofs-simple}}$ [NR]

model. The common-midpoint gather is a hyperbola whose asymptotes are straight lines with slopes of the inverse of the velocity v_1. The most basic data processing is called *common-depth-point stack* or CDP stack. In it, all the traces on the common-midpoint (CMP) gather are time shifted into alignment and then added together. The result mimics a zero-offset trace. The collection of all such traces is called the *CDP-stacked section.* In practice the CDP-stacked section is often interpreted and migrated as though it were a zero-offset section. In this chapter we will learn to avoid this popular, oversimplified assumption.

The next simplest environment is to have a planar reflector that is oriented vertically rather than horizontally. This is not typical, but is included here because the effect of earth dip is more comprehensible in an extreme case. Now the wave propagation is along the air-earth interface. To avoid confusion the reflector may be inclined at a slight angle from the vertical, as in Figure 1.13.

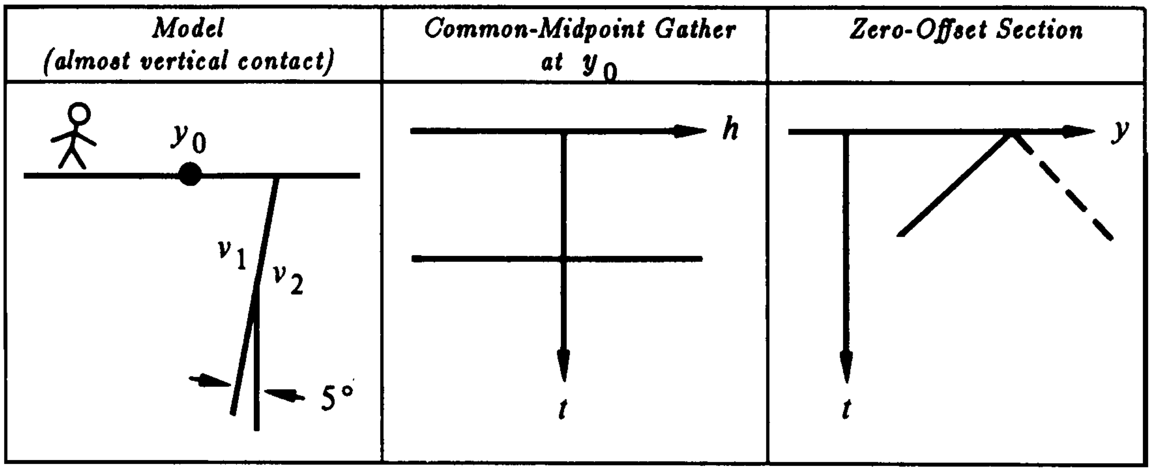

Figure 6.13: Near-vertical reflector, a gather, and a section. ofs-vertlay [NR]

Figure 1.13 shows that the travel time does not change as the offset changes. It may seem paradoxical that the travel time does not increase as the shot and geophone get further apart. The key to the paradox is that midpoint is held constant, not shotpoint. As offset increases, the shot gets further from the reflector while the geophone gets closer. Time lost on one path is gained on the other.

A planar reflector may have any dip between horizontal and vertical. Then the common-midpoint gather lies between the common-midpoint gather of Figure 1.12 and that of Figure 1.13. The zero-offset section in Figure 1.13 is a straight line, which turns out to be the asymptote of a family of hyperbolas. The slope of the asymptote is the inverse of the velocity v_1.

6.2.2 The dipping bed

While the travel-time curves resulting from a dipping bed are simple, they are not simple to derive. Before the derivation, the result will be stated: for a bed dipping at angle α from the horizontal, the travel-time curve is

$$t^2\,v^2 \quad = \quad 4\,(y-y_0)^2\,\sin^2\alpha \;+\; 4\,h^2\,\cos^2\alpha \tag{6.3}$$

For $\alpha = 45°$, equation (1.3) is the familiar Pythagoras cone—it is just like $t^2 = z^2 + x^2$. For other values of α, the equation is still a cone, but a less familiar one because of the stretched axes.

For a common-midpoint gather at $y = y_1$ in (h,t)-space, equation (1.3) looks like $t^2 = t_0^2 + 4h^2/v^2_{\text{apparent}}$. Thus the common-midpoint gather contains an *exact* hyperbola, regardless of the earth dip angle α. The effect of dip is to change the asymptote of the hyperbola, thus changing the apparent velocity. The result has great significance in applied work and is known as Levin's dip correction [1971]:

$$v_{\text{apparent}} \quad = \quad \frac{v_{\text{earth}}}{\cos(\alpha)} \tag{6.4}$$

(See also Slotnick [1959]). In summary, dip increases the stacking velocity.

Figure 1.14 depicts some rays from a common-midpoint gather. Notice that each

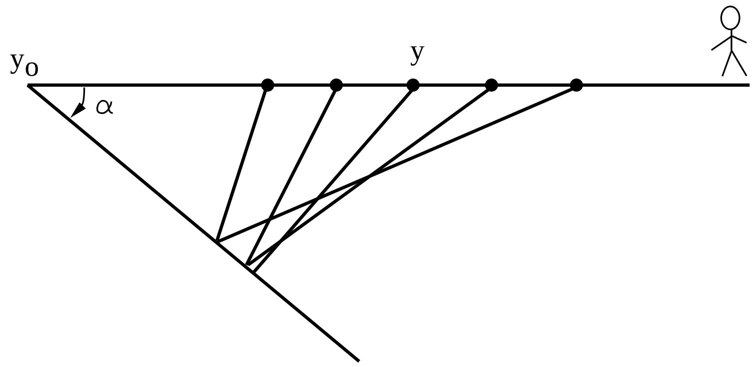

Figure 6.14: Rays from a common-midpoint gather. ofs-dipray [NR]

ray strikes the dipping bed at a different place. So a common-*midpoint* gather is not a common-*depth-point* gather. To realize why the reflection point moves on the reflector, recall the basic geometrical fact that an angle bisector in a triangle generally doesn't bisect the opposite side. The reflection point moves *up* dip with increasing offset.

Finally, equation (1.3) will be proved. Figure 1.15 shows the basic geometry along with an "image" source on another reflector of twice the dip. For convenience, the bed intercepts the surface at $y_0 = 0$. The length of the line $s'g$ in Figure 1.15 is

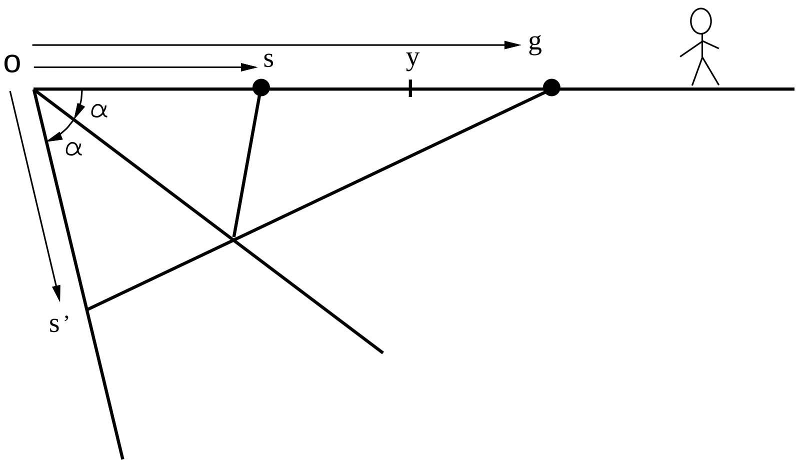

Figure 6.15: Travel time from image source at s' to g may be expressed by the law of cosines. ofs-lawcos [NR]

determined by the trigonometric Law of Cosines to be

$$\begin{aligned}
t^2 v^2 &= s^2 + g^2 - 2 s g \cos 2\alpha \\
t^2 v^2 &= (y - h)^2 + (y + h)^2 - 2 (y - h)(y + h) \cos 2\alpha \\
t^2 v^2 &= 2 (y^2 + h^2) - 2 (y^2 - h^2) (\cos^2 \alpha - \sin^2 \alpha) \\
t^2 v^2 &= 4 y^2 \sin^2 \alpha + 4 h^2 \cos^2 \alpha
\end{aligned}$$

which is equation (1.3).

Another facet of equation (1.3) is that it describes the constant-offset section. Surprisingly, the travel time of a dipping planar bed becomes curved at nonzero offset—it too becomes hyperbolic.

6.2.3 The point response

Another simple geometry is a reflecting point within the earth. A wave incident on the point from any direction reflects waves in all directions. This geometry is particularly important because any model is a superposition of such point scatterers. Figure 1.16 shows an example. The curves in Figure 1.16 include flat spots for the same reasons that some of the curves in figures1.12 and 1.13 were straight lines.

The point-scatterer geometry for a point located at (x, z) is shown in Figure 1.17.

The equation for travel time t is the sum of the two travel paths

$$t v = \sqrt{z^2 + (s - x)^2} + \sqrt{z^2 + (g - x)^2} \tag{6.5}$$

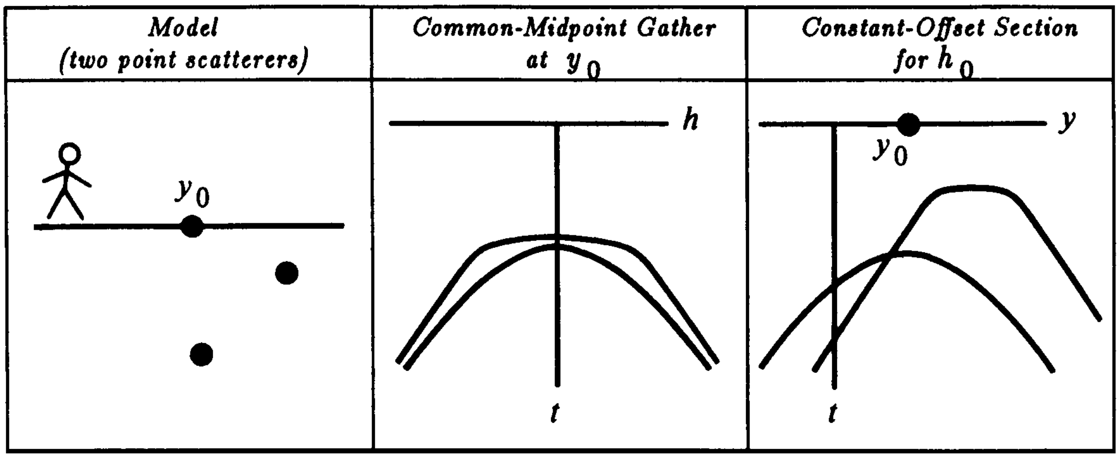

Figure 6.16: Response of two point scatterers. Note the flat spots. ofs-twopoint [NR]

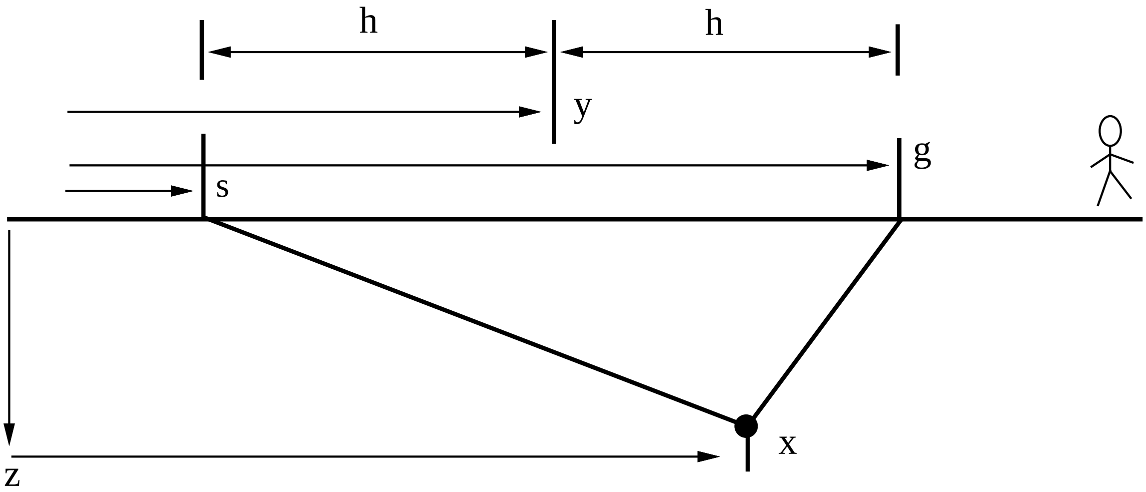

Figure 6.17: Geometry of a point scatterer. ofs-pgeometry [NR]

6.2.4 Cheops' pyramid

Because of the importance of the point-scatterer model, we will go to considerable lengths to visualize the functional dependence among t, z, x, s, and g in equation (1.5). This picture is more difficult—by one dimension—than is the conic section of the exploding-reflector geometry.

To begin with, suppose that the first square root in (1.5) is constant because everything in it is held constant. This leaves the familiar hyperbola in (g, t)-space, except that a constant has been added to the time. Suppose instead that the other square root is constant. This likewise leaves a hyperbola in (s, t)-space. In (s, g)-space, travel time is a function of s plus a function of g. I think of this as one coat hanger, which is parallel to the s-axis, being hung from another coat hanger, which is parallel to the g-axis.

A view of the travel-time pyramid on the (s, g)-plane or the (y, h)-plane is shown in Figure 1.18a. Notice that a cut through the pyramid at large t is a square, the corners

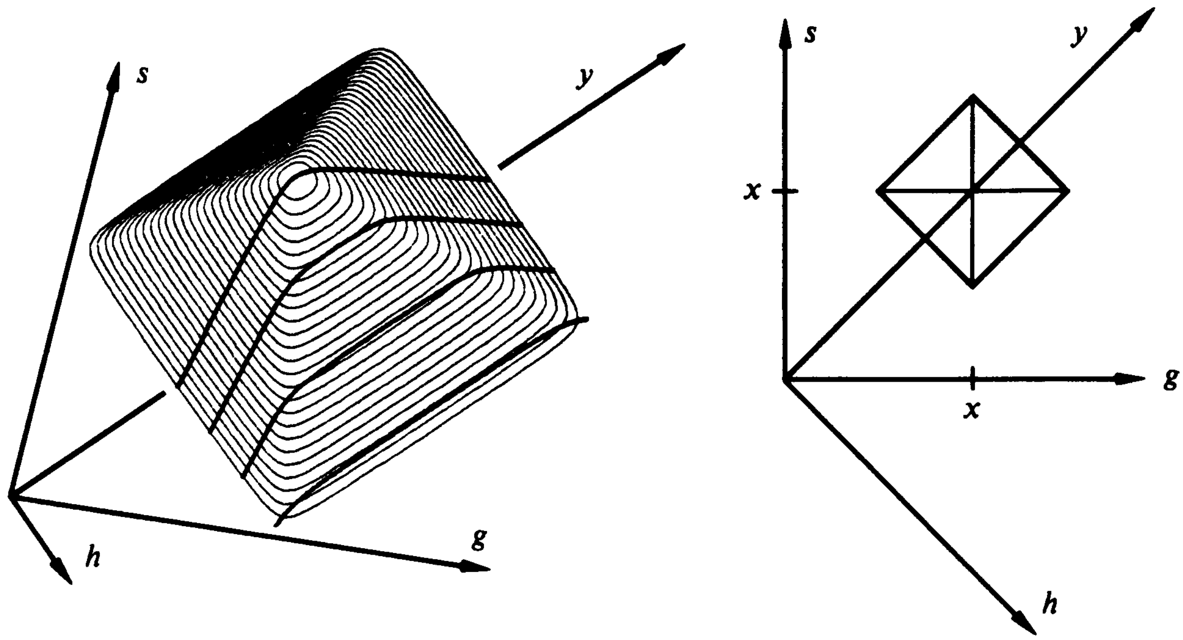

Figure 6.18: Left is a picture of the travel-time pyramid of equation ?? for fixed x and z. The darkened lines are constant-offset sections. Right is a cross section through the pyramid for large t (or small z). (Ottolini) ofs-cheop [NR]

of which have been smoothed. At very large t, a constant value of t is the square contoured in (s, g)-space, as in Figure 1.18b. Algebraically, the squareness becomes evident for a point reflector near the surface, say, $z \to 0$. Then (1.5) becomes

$$v\,t \quad = \quad |s \,-\, x| \;+\; |g \,-\, x| \tag{6.6}$$

The center of the square is located at $(s, g) = (x, x)$. Taking travel time t to increase downward from the horizontal plane of (s, g)-space, the square contour is like a horizontal slice through the Egyptian pyramid of Cheops. To walk around the pyramid at a constant altitude is to walk around a square. Alternately, the altitude change of a traverse over g at constant s is simply a constant plus an absolute-value function, as is a traverse of s at constant g.

More interesting and less obvious are the curves on common-midpoint gathers and constant-offset sections. Recall the definition that the midpoint between the shot and geophone is y. Also recall that h is half the horizontal offset from the shot to the geophone.

$$y = \frac{g + s}{2} \tag{6.7}$$

$$h = \frac{g - s}{2} \tag{6.8}$$

A traverse of y at constant h is shown in Figure 1.18. At the highest elevation on the traverse, you are walking along a flat horizontal step like the flat-topped hyperboloids of Figure 1.16. Some erosion to smooth the top and edges of the pyramid gives a model for nonzero reflector depth.

For rays that are near the vertical, the travel-time curves are far from the hyperbola asymptotes. Then the square roots in (1.5) may be expanded in Taylor series, giving a parabola of revolution. This describes the eroded peak of the pyramid.

6.2.5 Random point scatterers

Figure 1.19 shows a synthetic constant-offset section (COS) taken from an earth model containing about fifty randomly placed point scatterers. Late arrival times

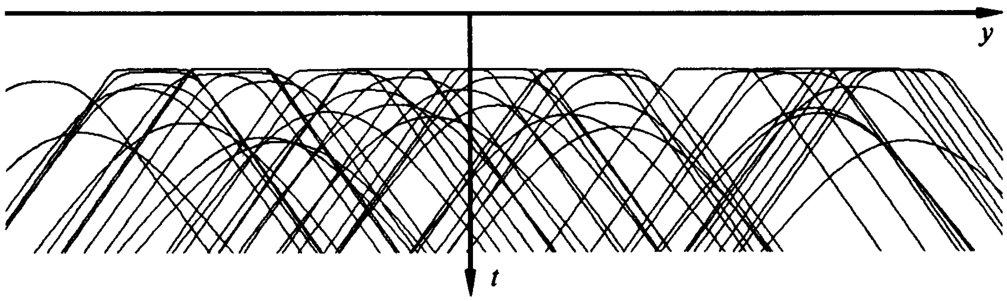

Figure 6.19: Constant-offset section over random point scatterers. $\boxed{\text{ofs-randcos}}$ [NR]

appear hyperbolic. Earlier arrivals have flattened tops. The earliest possible arrival corresponds to a ray going horizontally from the shot to the geophone.

Figure 1.20 shows a synthetic common-shot profile (CSP) from the same earth model of random point scatterers. Each scatterer produces a hyperbolic arrival. The hyperbolas are not symmetric around zero offset; their locations are random. They

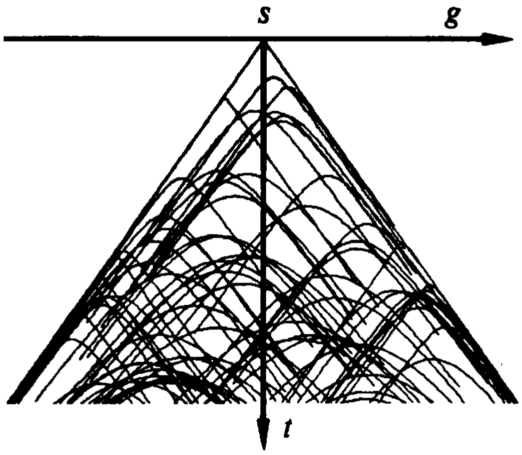

Figure 6.20: Common-shot profile over random point scatterers. ofs-randcsp [NR]

must, however, all lie under the lines $|g - s| = vt$. Hyperbolas with sharp tops can be found at late times as well as early times. However, the sharp tops, which are from shallow scatterers near the geophone, must lie near the lines $|g - s| = vt$.

The left side of Figure 1.21 shows a synthetic common-midpoint gather (CMP) from an earth model containing about fifty randomly placed point scatterers. Because

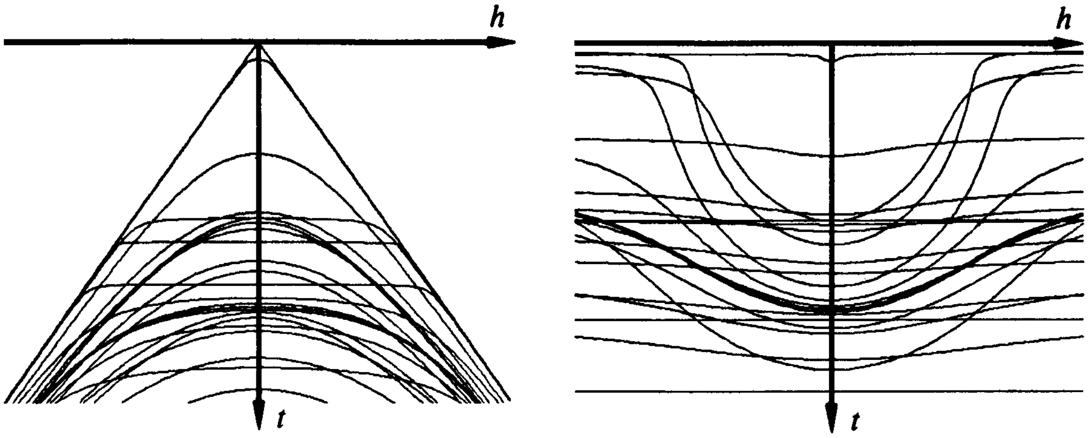

Figure 6.21: Common-midpoint gather on earth of randomly located point scatterers (left). The same gathers after NMO correction (right). ofs-randcmp [NR]

this is a common-*midpoint* gather, the curves are symmetric through zero offset. (The negative offsets of field data are hardly ever plotted). Some of the arrivals have flattened tops, which indicate scatterers that are not directly under the midpoint.

Normal-moveout (NMO) correction is a stretching of the data to try to flatten the hyperbolas. This correction assumes flat beds, but it also works for point scatterers that are directly under the midpoint. The right side of Figure 1.21 shows what happens when normal-moveout correction is applied on the random scatterer model. Some reflectors are flattened; others are “overcorrected.”

6.2.6 Forward and backward scattering: Larner's streaks

At some locations, near-surface waves overwhelm the deep reflections of geologic interest. Compounding our difficulty, the near-surface waves are usually irregular because the earth is comparatively more irregular at its surface than deeper down. On land, these interfering waves are called ground roll. At sea, they are called water waves (not to be confused with surface waves on water).

A model for such near-surface noises is suggested by the vertical reflecting wall in Figure 1.13. In this model the waves remain close to the surface. Randomly placed vertical walls could result in a zero-offset section that resembles the field data of Figure 1.22. Another less extreme model for the surface noises is the flat-topped curves in the random point-scatterer model.

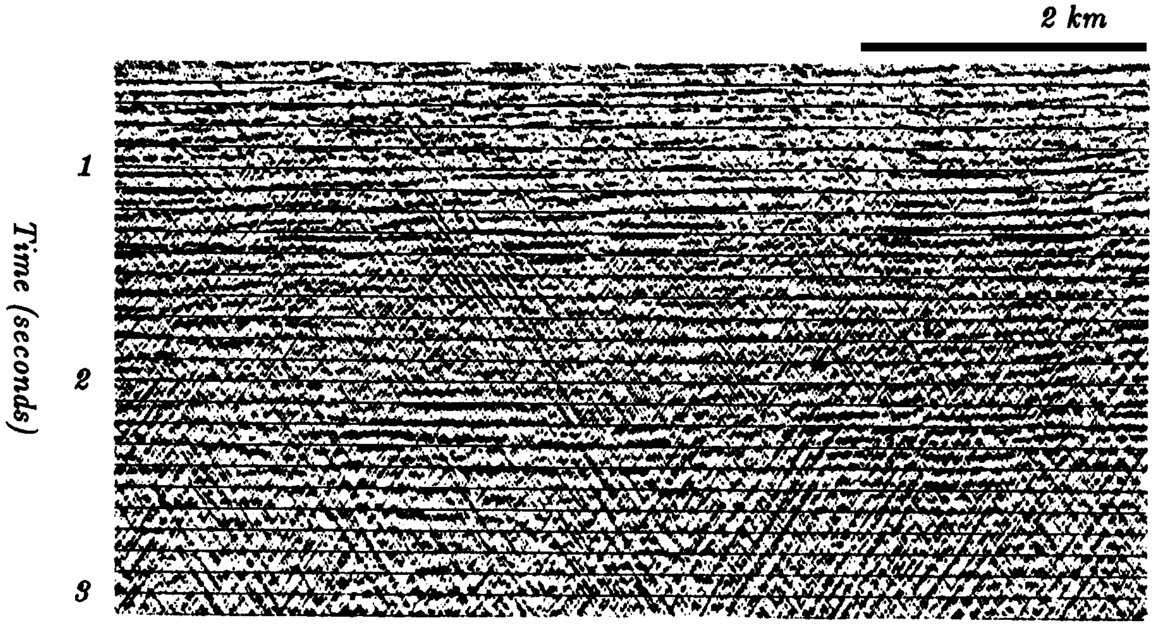

Figure 6.22:)
] CDP stack with water noise from the Shelikof Strait, Alaska. (by permission from *Geophysics,* Larner et al. [1983]) $\boxed{\text{ofs-shelikof}}$ [NR]

In the random point-reflector model the velocity was a constant. In real life the earth velocity is generally slower for the near-surface waves and faster for the deep reflections. This sets the stage for some unexpected noise amplification.

CDP stacking enhances events with the stacking velocity and discriminates against events with other velocities. Thus you might expect that stacking at deeper, higher velocity would discriminate against low-velocity, near-surface events. Near-surface noises, however, are not reflections from horizontal layers; they are more like reflections from vertical walls or steeply dipping layers. But equation (1.4) shows that dip increases the apparent velocity. So it is not surprising that stacking at deep-sediment, high velocities can enhance surface noises. Occurrence of this problem in practice was nicely explained and illustrated by Larner et al. [1983]

6.2.7 Velocity of sideswipe

Shallow-water noise can come from waves scattering from a sunken ship or from the side of an island or iceberg several kilometers to the side of the survey line. Think of boulders strewn all over a shallow sea floor, not only along the path of the ship, but also off to the sides. (Reality is more impressive. Wind blown ice flows drag themselves along the bottom making huge scars in it.) The travel-time curves for reflections from the boulders nicely matches the random point-scatterer model. Because of the long wavelengths of seismic waves, our sending and receiving equipment does not enable us to distinguish waves going up and down from those going sideways.

Imagine one of these shallow scatterers several kilometers to the side of the ship. More precisely, let the scatterer be on the earth's surface, perpendicular to the midpoint of the line connecting the shot point to the geophone. A common-midpoint gather for this scatterer is a perfect hyperbola, as from the deep reflector contributions on Figure 1.20. Since it is a water-velocity hyperbola, this scatterered noise should be nicely suppressed by CDP stacking with the higher, sediment velocity. So the "streaking" scatterers in Figure 1.22 are not sidescatter.

The "streaking" scatterers are those neither along the survey line nor those perpendicular to it. The "in-line" scatterers have infinite velocity (on the flat spot). The scatterers perpendicular to the survey line have the water velocity. Scatterers at other angles have inbetween velocities and they stack strongly at the sediment velocity and account for the streaks.

6.2.8 The migration ellipse

Another insight into equation (1.5) is to regard the offset h and the total travel time t as fixed constants. Then the locus of possible reflectors turns out to describe an ellipse in the plane of $(y-y_0, z)$. The reason it is an ellipse follows from the geometric definition of an ellipse. To draw an ellipse, place a nail or tack into s on Figure 1.17 and another into g. Connect the tacks by a string that is exactly long enough to go through (y_0, z). An ellipse going through (y_0, z) may be constructed by sliding a pencil along the string, keeping the string tight. The string keeps the total distance tv constant.

Recall that one method for migrating zero-offset sections is to take every data value in (y, t)-space and use it to superpose an appropriate semicircle in (y, z)-space. For nonzero offset the circle should be generalized to an ellipse (Figure 3.6).

It is not easy to show that equation (1.5) can be cast in the standard mathematical form of an ellipse, namely, a stretched circle. But the result is a simple one, and an important one for later analysis, so here we go. Equation (1.5) in (y, h)-space is

$$t\,v \quad = \quad \sqrt{z^2 \;+\; (y \;-\; y_0 \;-\; h)^2} \;+\; \sqrt{z^2 \;+\; (y \;-\; y_0 \;+\; h)^2} \tag{6.9}$$

To help reduce algebraic verbosity, define a new y equal to the old one shifted by y_0. Also make the definitions

$$\begin{aligned} t\,v_{\text{rock}} &= 2\,d \;=\; 2\,t\,v_{\text{half}} & (6.10)\\ a &= z^2 \;+\; (y \;+\; h)^2 & (6.11)\\ b &= z^2 \;+\; (y \;-\; h)^2 & (6.12)\\ a \;-\; b &= 4\,y\,h & (6.13) \end{aligned}$$

With these definitions, (1.9) becomes

$$2\,d \quad = \quad \sqrt{a} \;+\; \sqrt{b} \tag{6.14}$$

Square to get a new equation with only one square root.

$$4\,d^2 \;-\; (a \;+\; b) \quad = \quad 2\,\sqrt{a}\sqrt{b} \tag{6.15}$$

Square again to eliminate the square root.

$$\begin{aligned} 16\,d^4 \;-\; 8\,d^2\,(a \;+\; b) \;+\; (a \;+\; b)^2 &= 4\,a\,b & (6.16)\\ 16\,d^4 \;-\; 8\,d^2\,(a \;+\; b) \;+\; (a \;-\; b)^2 &= 0 & (6.17) \end{aligned}$$

Introduce definitions of a and b.

$$16\,d^4 \;-\; 8\,d^2\,[\,2\,z^2 \;+\; 2\,y^2 \;+\; 2\,h^2] \;+\; 16\,y^2\,h^2 \quad = \quad 0 \tag{6.18}$$

Bring y and z to the right.

$$\begin{aligned} d^4 \;-\; d^2\,h^2 &= d^2\,(z^2 \;+\; y^2) \;-\; y^2\,h^2 & (6.19)\\ d^2\,(d^2 \;-\; h^2) &= d^2\,z^2 \;+\; (d^2 \;-\; h^2)\,y^2 & (6.20)\\ d^2 &= \frac{z^2}{1 \;-\; \frac{h^2}{d^2}} \;+\; y^2 & (6.21) \end{aligned}$$

Finally, recalling all earlier definitions,

$$t^2\;v_{\text{half}}^2 \quad = \quad \frac{z^2}{1 \;-\; \frac{h^2}{t^2\;v_{\text{half}}^2}} \;+\; (y \;-\; y_0)^2 \tag{6.22}$$

Fixing t, equation (1.22) is the equation for a circle with a stretched z-axis. Our algebra has confirmed that the "string and tack" definition of an ellipse matches the "stretched circle" definition. An ellipse in model space is the earth model given the observation of an impulse on a constant-offset section.

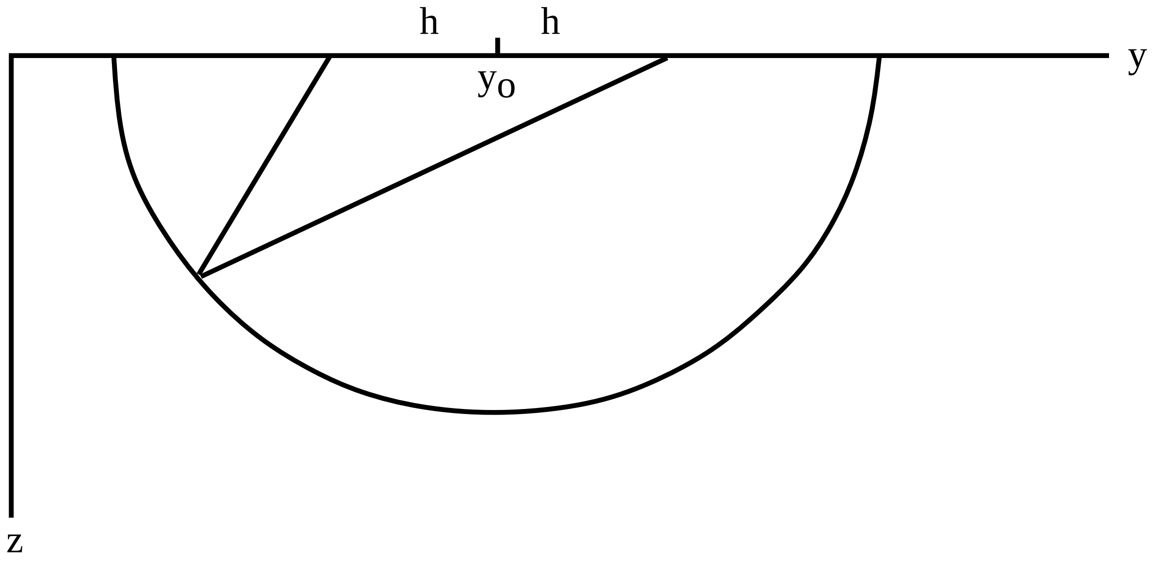

Figure 6.23: Migration ellipse. ofs-ellipse [NR]

6.3 SURVEY SINKING WITH THE DOUBLE-SQUARE-ROOT EQUATION

Exploding-reflector imaging will be replaced by a broader imaging concept, *survey sinking.* A new equation called the double-square-root (DSR) equation will be developed to implement survey-sinking imaging. The function of the DSR equation is to downward continue an entire seismic survey, not just the geophones but also the shots. After deriving the DSR equation, the remainder of this chapter will be devoted to explaining migration, stacking, migration before stack, velocity analysis, and corrections for lateral velocity variations in terms of the DSR equation.

Peek ahead at equation (1.35) and you will see an equation with two square roots. One represents the cosine of the wave *arrival* angle. The other represents the *takeoff* angle at the shot. One cosine is expressed in terms of k_g, the Fourier component along the geophone axis of the data volume in (s, g, t)-space. The other cosine, with k_s, is the Fourier component along the shot axis.

Our field seismograms lie in the (s, g)-plane. To move onto the (y, h)-plane inhabited by seismic interpreters requires only a simple rotation. The data could be Fourier transformed with respect to y and h, for example. Then downward continuation would proceed with equation (1.48) instead of equation (1.35).

The DSR equation depends upon the reciprocity principle which we will review first.

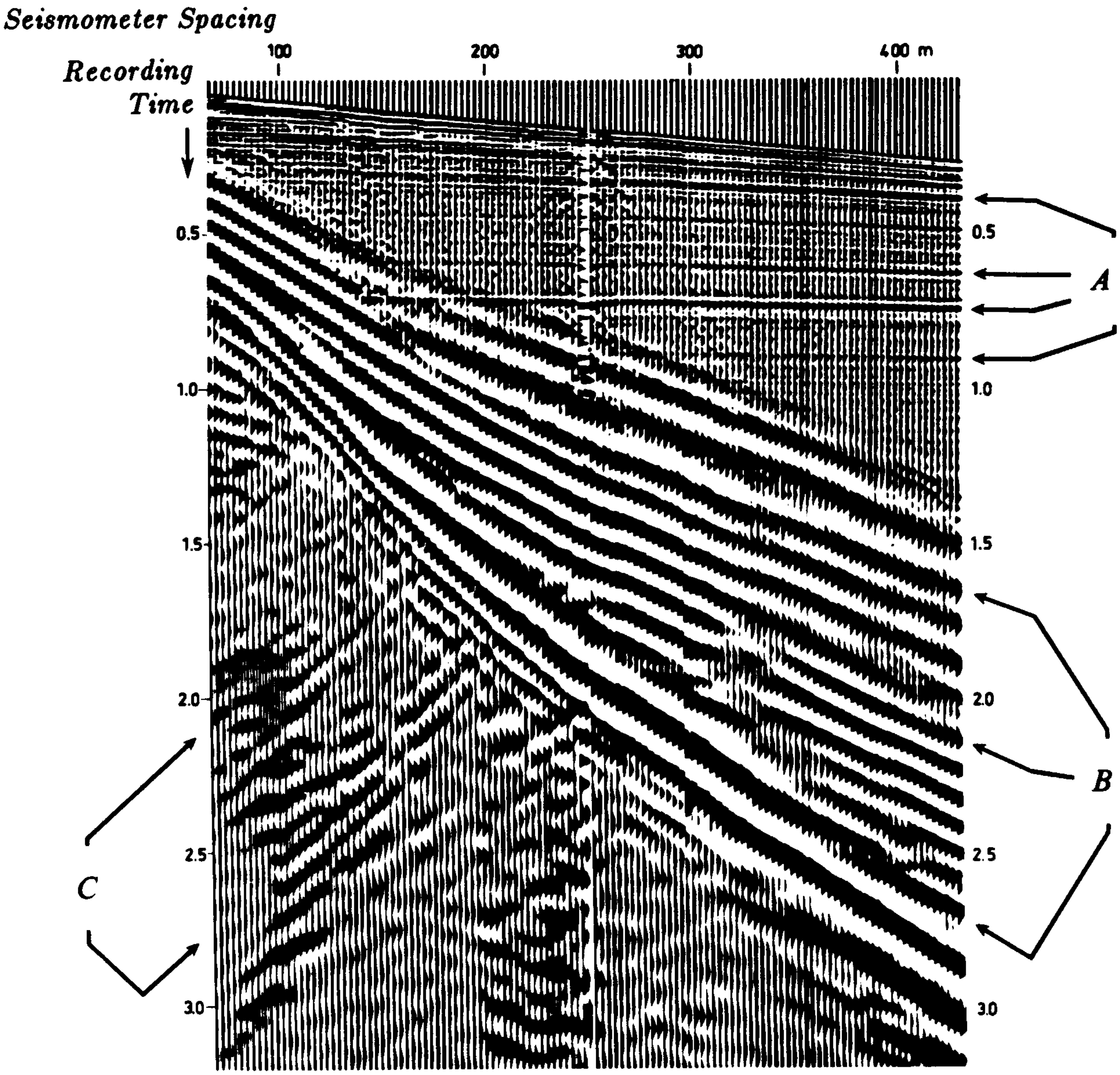

Figure 6.24: Undocumented data from a recruitment brochure. This data may be assumed to be of textbook quality. The speed of sound in water is about 1500 m/sec. Identify the events at A, B, and C. Is this a common-shotpoint gather or a common-midpoint gather? (Shell Oil Company) $\boxed{\text{ofs-shell}}$ [NR]

6.3.1 Seismic reciprocity in principle and in practice

The principle of reciprocity says that the same seismogram should be recorded if the locations of the source and geophone are exchanged. A physical reason for the validity of reciprocity is that no matter how complicated a geometrical arrangement, the speed of sound along a ray is the same in either direction.

Mathematically, the reciprocity principle arises because the physical equations of elasticity are self adjoint. The meaning of the term *self adjoint* is illustrated in FGDP where it is shown that discretized acoustic equations yield a *symmetric* matrix even where density and compressibility are space variable. The inverse of any such symmetric matrix is another symmetric matrix called the impulse-response matrix. Elements across the matrix diagonal are equal to one another. Each element of any pair is a response to an impulsive source. The opposite element of the pair refers to the interchanged source and receiver.

A tricky thing about the reciprocity principle is the way antenna patterns must be handled. For example, a single vertical geophone has a natural antenna pattern. It cannot see horizontally propagating pressure waves nor vertically propagating shear waves. For reciprocity to be applicable, antenna patterns must not be interchanged when source and receiver are interchanged. The antenna pattern must be regarded as attached to the medium.

I searched our data library for split-spread land data that would illustrate reciprocity under field conditions. The constant-offset section in Figure 1.25 was recorded by vertical vibrators into vertical geophones. The survey was not intended to be a test of reciprocity, so there likely was a slight lateral offset of the source line from the receiver line. Likewise the sender and receiver arrays (clusters) may have a slightly different geometry. The earth dips in Figure 1.25 happen to be quite small although lateral velocity variation is known to be a problem in this area.

In Figure 1.26, three seismograms were plotted on top of their reciprocals. Pairs were chosen at near offset, at mid range, and at far offset. You can see that reciprocal seismograms usually have the same polarity, and often have nearly equal amplitudes. (The figure shown is the best of three such figures I prepared).

Each constant time slice in Figure 1.27 shows the reciprocity of many seismogram pairs. Midpoint runs horizontally over the same range as in Figure 1.25. Offset is vertical. Data is not recorded near the vibrators leaving a gap in the middle. To minimize irrelevant variations, moveout correction was done before making the time slices. (There is a missing source that shows up on the left side of the figure). A movie of panels like Figure 1.27 shows that the bilateral symmetry you see in the individual panels is characteristic of all times. Notice however that there is a significant departure from reciprocity on the one-second time slice around midpoint 120.

In the laboratory, reciprocity can be established to within the accuracy of measurement. This can be excellent. (See White's example in FGDP). In the field,

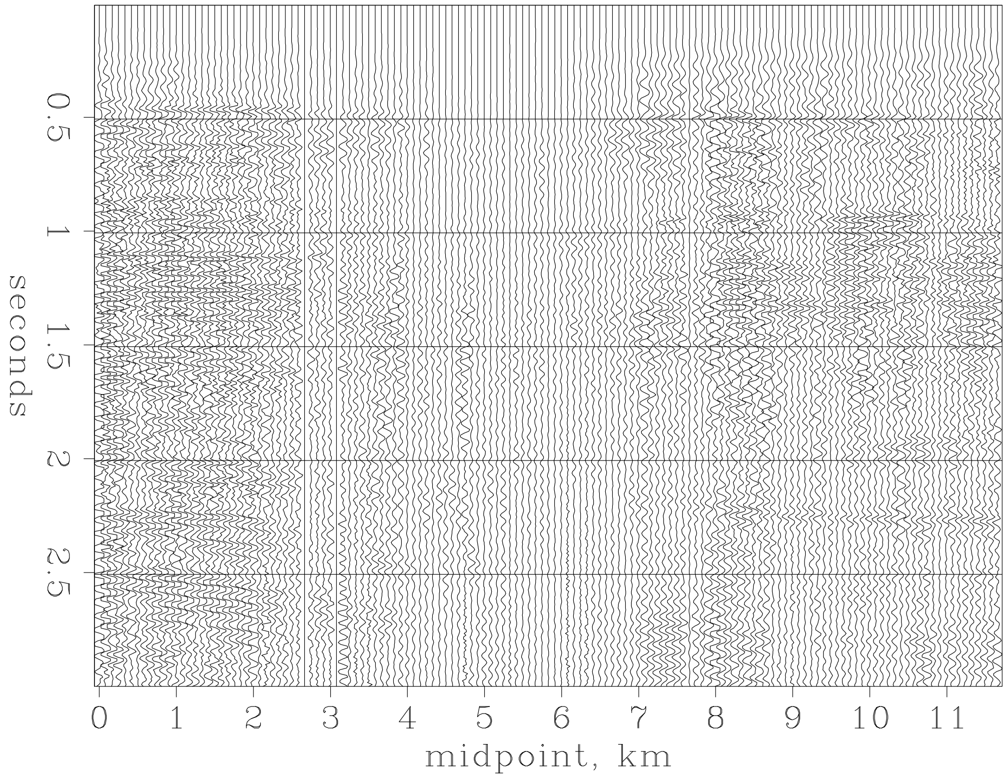

Figure 6.25: Constant-offset section from the Central Valley of California. (Chevron) ofs-toldi [ER]

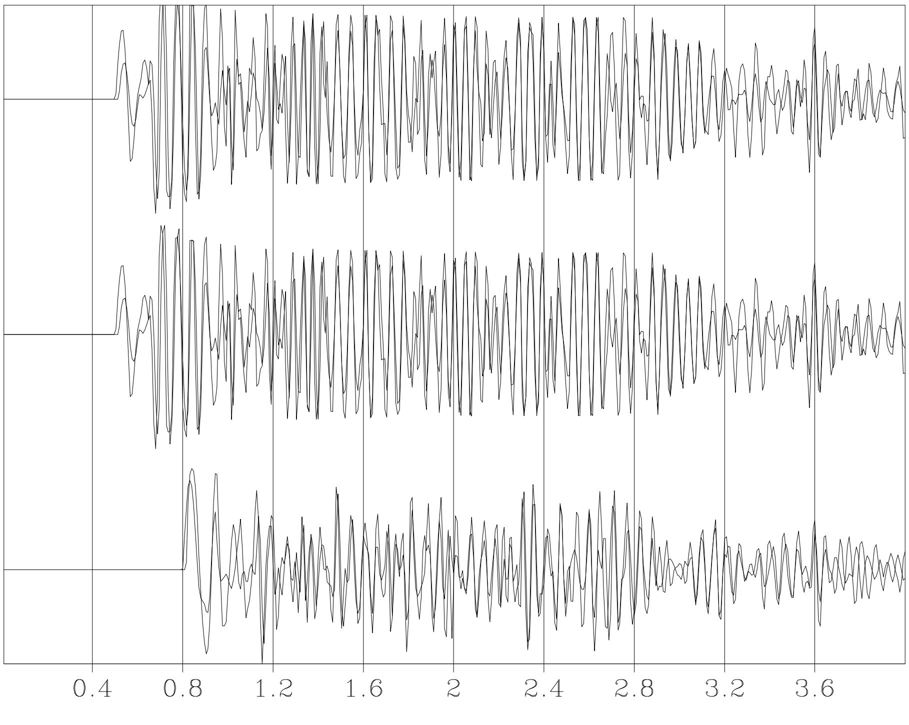

Figure 6.26: Overlain reciprocal seismograms. ofs-reciptrace [ER]

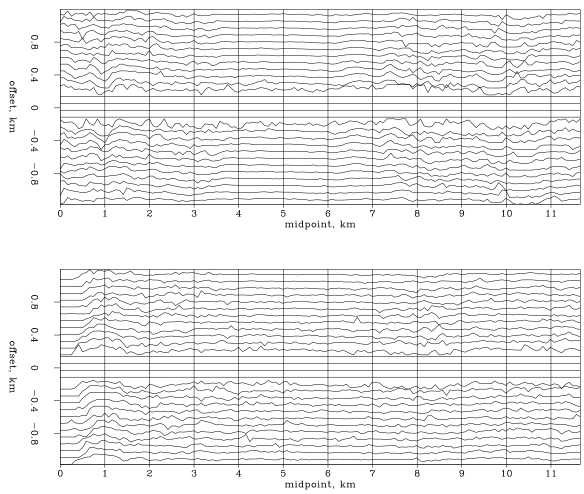

Figure 6.27: Constant time slices after NMO at 1 second and 2.5 seconds. ofs-recipslice [ER]

the validity of reciprocity will be dependent on the degree that the required conditions are fulfilled. A marine air gun should be reciprocal to a hydrophone. A land-surface weight-drop source should be reciprocal to a vertical geophone. But a buried explosive shot need not be reciprocal to a surface vertical geophone because the radiation patterns are different and the positions are slightly different. Fenati and Rocca [1984] studied reciprocity under varying field conditions. They reported that small positioning errors in the placement of sources and receivers can easily create discrepancies larger than the apparent reciprocity discrepancy. They also reported that theoretically reciprocal experiments may actually be less reciprocal than presumably nonreciprocal experiments.

Geometrical complexity within the earth does not diminish the applicability of the principle of linearity. Likewise, geometrical complexity does not reduce the applicability of reciprocity. Reciprocity does not apply to sound waves in the presence of wind. Sound goes slower upwind than downwind. But this effect of wind is much less than the mundane irregularities of field work. Just the weakening of echoes with time leaves noises that are not reciprocal. Henceforth we will presume that reciprocity is generally applicable to the analysis of reflection seismic data.

6.3.2 The survey-sinking concept

The exploding-reflector concept has great utility because it enables us to associate the seismic waves observed at zero offset in many experiments (say 1000 shot points) with the wave of a single thought experiment, the exploding-reflector experiment. The exploding-reflector analogy has a few tolerable limitations connected with lateral velocity variations and multiple reflections, and one major limitation: it gives us no clue as to how to migrate data recorded at nonzero offset. A broader imaging concept is needed.

Start from field data where a survey line has been run along the x-axis. Assume there has been an infinite number of experiments, a single experiment consisting of placing a point source or shot at s on the x-axis and recording echoes with geophones at each possible location g on the x-axis. So the observed data is an upcoming wave that is a two-dimensional function of s and g, say $P(s, g, t)$.

Previous chapters have shown how to downward continue the *upcoming* wave. Downward continuation of the upcoming wave is really the same thing as downward continuation of the geophones. It is irrelevant for the continuation procedures where the wave originates. It could begin from an exploding reflector, or it could begin at the surface, go down, and then be reflected back upward.

To apply the imaging concept of survey sinking, it is necessary to downward continue the sources as well as the geophones. We already know how to downward continue geophones. Since reciprocity permits interchanging geophones with shots, we really know how to downward continue shots too.

Shots and geophones may be downward continued to different levels, and they may be at different levels during the process, but for the final result they are only required to be at the same level. That is, taking z_s to be the depth of the shots and z_g to be the depth of the geophones, the downward-continued survey will be required at all levels $z = z_s = z_g$.

The image of a reflector at (x, z) is defined to be the strength and polarity of the echo seen by the closest possible source-geophone pair. Taking the mathematical limit, this closest pair is a source and geophone located together on the reflector. The travel time for the echo is zero. This survey-sinking concept of imaging is summarized by

$$\text{Image}(x, z) \quad = \quad \text{Wave}(s = x, g = x, z, t = 0) \tag{6.23}$$

For good quality data, i.e. data that fits the assumptions of the downward-continuation method, energy should migrate to zero offset at zero travel time. Study of the energy that doesn't do so should enable improvement of the model. Model improvement usually amounts to improving the spatial distribution of velocity.

6.3.3 Review of the paraxial wave equation

An equation was derived for paraxial waves. The assumption of a *single* plane wave means that the arrival time of the wave is given by a single-valued $t(x, z)$. On a plane of constant z, such as the earth's surface, Snell's parameter p is measurable. It is

$$\frac{\partial t}{\partial x} \quad = \quad \frac{\sin\,\theta}{v} \quad = \quad p \tag{6.24}$$

In a borehole there is the constraint that measurements must be made at a constant x, where the relevant measurement from an *upcoming* wave would be

$$\frac{\partial t}{\partial z} \quad = \quad - \frac{\cos\theta}{v} \quad = \quad - \sqrt{\frac{1}{v^2} - \left(\frac{\partial t}{\partial x}\right)^2} \tag{6.25}$$

Recall the time-shifting partial-differential equation and its solution U as some arbitrary functional form f:

$$\frac{\partial U}{\partial z} \quad = \quad - \frac{\partial t}{\partial z}\frac{\partial U}{\partial t} \tag{6.26}$$

$$U \quad = \quad f\left(t - \int_0^z \frac{\partial t}{\partial z}\, dz \right) \tag{6.27}$$

The partial derivatives in equation (1.26) are taken to be at constant x, just as is equation (1.25). After inserting (1.25) into (1.26) we have

$$\frac{\partial U}{\partial z} \quad = \quad \sqrt{\frac{1}{v^2} - \left(\frac{\partial t}{\partial x}\right)^2}\ \frac{\partial U}{\partial t} \tag{6.28}$$

Fourier transforming the wavefield over (x, t), we replace $\partial/\partial t$ by $-i\omega$. Likewise, for the traveling wave of the Fourier kernel $\exp(-i\omega t + ik_x x)$, constant phase means that $\partial t/\partial x = k_x/\omega$. With this, (1.28) becomes

$$\frac{\partial U}{\partial z} \quad = \quad -i\omega\sqrt{\frac{1}{v^2} - \frac{k_x^2}{\omega^2}}\ U \tag{6.29}$$

The solutions to (1.29) agree with those to the scalar wave equation unless v is a function of z, in which case the scalar wave equation has both upcoming and downgoing solutions, whereas (1.29) has only upcoming solutions. Chapter 4 taught us how to go into the lateral space domain by replacing ik_x by $\partial/\partial x$. The resulting equation is useful for superpositions of many local plane waves and for lateral velocity variations $v(x)$.

6.3.4 The DSR equation in shot-geophone space

Let the geophones descend a distance dz_g into the earth. The change of the travel time of the observed upcoming wave will be

$$\frac{\partial t}{\partial z_g} \quad = \quad - \sqrt{\frac{1}{v^2} - \left(\frac{\partial t}{\partial g}\right)^2} \tag{6.30}$$

Suppose the shots had been let off at depth dz_s instead of at $z = 0$. Likewise then,

$$\frac{\partial t}{\partial z_s} \quad = \quad - \sqrt{\frac{1}{v^2} - \left(\frac{\partial t}{\partial s}\right)^2} \tag{6.31}$$

Both (1.30) and (1.31) require minus signs because the travel time decreases as either geophones or shots move down.

Simultaneously downward project both the shots and geophones by an identical vertical amount $dz = dz_g = dz_s$. The travel-time change is the sum of (1.30) and (1.31), namely,

$$dt \quad = \quad \frac{\partial t}{\partial z_g}\, dz_g \;+\; \frac{\partial t}{\partial z_s}\, dz_s \quad = \quad \left(\frac{\partial t}{\partial z_g} \;+\; \frac{\partial t}{\partial z_s} \right)\, dz \tag{6.32}$$

or

$$\frac{\partial t}{\partial z} \quad = \quad -\left(\sqrt{\frac{1}{v^2} \,-\, \left(\frac{\partial t}{\partial g}\right)^2} \;+\; \sqrt{\frac{1}{v^2} \,-\, \left(\frac{\partial t}{\partial s}\right)^2} \right) \tag{6.33}$$

This expression for $\partial t / \partial z$ may be substituted into equation (1.26):

$$\frac{\partial U}{\partial z} \quad = \quad +\left(\sqrt{\frac{1}{v^2} \,-\, \left(\frac{\partial t}{\partial g}\right)^2} \;+\; \sqrt{\frac{1}{v^2} \,-\, \left(\frac{\partial t}{\partial s}\right)^2} \right) \frac{\partial U}{\partial t} \tag{6.34}$$

Three-dimensional Fourier transformation converts upcoming wave data $u(t, s, g)$ to $U(\omega, k_s, k_g)$. Expressing equation (1.34) in Fourier space gives

$$\frac{\partial U}{\partial z} \quad = \quad -\,i\,\omega \left[\sqrt{\frac{1}{v^2} \,-\, \left(\frac{k_g}{\omega}\right)^2} \;+\; \sqrt{\frac{1}{v^2} \,-\, \left(\frac{k_s}{\omega}\right)^2} \right] U \tag{6.35}$$

Recall the origin of the two square roots in equation (1.35). One is the cosine of the arrival angle at the geophones divided by the velocity at the geophones. The other is the cosine of the takeoff angle at the shots divided by the velocity at the shots. With the wisdom of previous chapters we know how to go into the lateral space domain by replacing ik_g by $\partial/\partial g$ and ik_s by $\partial/\partial s$. To incorporate lateral velocity variation $v(x)$, the velocity at the shot location must be distinguished from the velocity at the geophone location. Thus,

$$\frac{\partial U}{\partial z} \quad = \quad \left[\sqrt{\left(\frac{-\,i\omega}{v}(g) \right)^2 \,-\, \frac{\partial^2}{\partial g^2}} \;+\; \sqrt{\left(\frac{-\,i\omega}{v}(s) \right)^2 \,-\, \frac{\partial^2}{\partial s^2}} \right] U \tag{6.36}$$

Equation (1.36) is known as the double-square-root (DSR) equation in shot-geophone space. It might be more descriptive to call it the survey-sinking equation since it pushes geophones and shots downward together. Recalling the section on splitting and full separation we realize that the two square-root operators are commutative ($v(s)$ commutes with $\partial/\partial g$), so it is completely equivalent to downward continue shots and geophones separately or together. This equation will produce waves for the rays that are found on zero-offset sections but are absent from the exploding-reflector model.

6.3.5 The DSR equation in midpoint-offset space

By converting the DSR equation to midpoint-offset space we will be able to identify the familiar zero-offset migration part along with corrections for offset. The transformation between (g, s) recording parameters and (y, h) interpretation parameters is

$$y \quad = \quad \frac{g \ + \ s}{2} \tag{6.37}$$

$$h \quad = \quad \frac{g \ - \ s}{2} \tag{6.38}$$

Travel time t may be parameterized in (g, s)-space or (y, h)-space. Differential relations for this conversion are given by the chain rule for derivatives:

$$\frac{\partial t}{\partial g} \quad = \quad \frac{\partial t}{\partial y}\frac{\partial y}{\partial g} + \frac{\partial t}{\partial h}\frac{\partial h}{\partial g} \quad = \quad \frac{1}{2}\left(\frac{\partial t}{\partial y} + \frac{\partial t}{\partial h}\right) \tag{6.39}$$

$$\frac{\partial t}{\partial s} \quad = \quad \frac{\partial t}{\partial y}\frac{\partial y}{\partial s} + \frac{\partial t}{\partial h}\frac{\partial h}{\partial s} \quad = \quad \frac{1}{2}\left(\frac{\partial t}{\partial y} - \frac{\partial t}{\partial h}\right) \tag{6.40}$$

Having seen how stepouts transform from shot-geophone space to midpoint-offset space, let us next see that spatial frequencies transform in much the same way. Clearly, data could be transformed from (s, g)-space to (y, h)-space with (1.37) and (1.38) and then Fourier transformed to (k_y, k_h)-space. The question is then, what form would the double-square-root equation (1.35) take in terms of the spatial frequencies (k_y, k_h)? Define the seismic data field in either coordinate system as

$$U(s, g) \quad = \quad U'(y, h) \tag{6.41}$$

This introduces a new mathematical function U' with the same physical meaning as U but, like a computer subroutine or function call, with a different subscript look-up procedure for (y, h) than for (s, g). Applying the chain rule for partial differentiation to (1.41) gives

$$\frac{\partial U}{\partial s} \quad = \quad \frac{\partial y}{\partial s}\frac{\partial U'}{\partial y} + \frac{\partial h}{\partial s}\frac{\partial U'}{\partial h} \tag{6.42}$$

$$\frac{\partial U}{\partial g} \quad = \quad \frac{\partial y}{\partial g}\frac{\partial U'}{\partial y} + \frac{\partial h}{\partial g}\frac{\partial U'}{\partial h} \tag{6.43}$$

and utilizing (1.37) and (1.38) gives

$$\frac{\partial U}{\partial s} \quad = \quad \frac{1}{2}\left(\frac{\partial U'}{\partial y} - \frac{\partial U'}{\partial h}\right) \tag{6.44}$$

$$\frac{\partial U}{\partial g} \quad = \quad \frac{1}{2}\left(\frac{\partial U'}{\partial y} + \frac{\partial U'}{\partial h}\right) \tag{6.45}$$

In Fourier transform space where $\partial/\partial x$ transforms to ik_x, equations (1.44) and (1.45), when i and $U = U'$ are cancelled, become

$$k_s \quad = \quad \frac{1}{2}\,(k_y \;-\; k_h) \tag{6.46}$$

$$k_g \quad = \quad \frac{1}{2}\,(k_y \;+\; k_h) \tag{6.47}$$

Equations (1.46) and (1.47) are Fourier representations of (1.44) and (1.45). Substituting (1.46) and (1.47) into (1.35) achieves the main purpose of this section, which is to get the double-square-root migration equation into midpoint-offset coordinates:

$$\frac{\partial}{\partial z}\,U \quad = \quad -\,i\,\frac{\omega}{v}\left[\sqrt{1\;-\;\left(\frac{vk_y\;+\;vk_h}{2\,\omega}\right)^2}\;+\sqrt{1\;-\;\left(\frac{vk_y\;-\;vk_h}{2\,\omega}\right)^2}\;\right]\;U \tag{6.48}$$

Equation (1.48) is the takeoff point for many kinds of common-midpoint seismogram analyses. Some convenient definitions that simplify its appearance are

$$G \quad = \quad \frac{v\;k_g}{\omega} \tag{6.49}$$

$$S \quad = \quad \frac{v\;k_s}{\omega} \tag{6.50}$$

$$Y \quad = \quad \frac{v\;k_y}{2\;\omega} \tag{6.51}$$

$$H \quad = \quad \frac{v\;k_h}{2\;\omega} \tag{6.52}$$

Chapter 3 showed that the quantity $v\,k_x/\omega$ can be interpreted as the angle of a wave. Thus the new definitions S and G are the sines of the takeoff angle and of the arrival angle of a ray. When these sines are at their limits of ± 1 they refer to the steepest possible slopes in (s,t)- or (g,t)-space. Likewise, Y may be interpreted as the dip of the data as seen on a seismic section. The quantity H refers to stepout observed on a common-midpoint gather. With these definitions (1.48) becomes slightly less cluttered:

$$\boxed{\frac{\partial}{\partial z}U \quad = \quad -\frac{i\omega}{v}\left(\sqrt{1-(Y+H)^2}+\sqrt{1-(Y-H)^2}\;\right)U} \tag{6.53}$$

Most present-day before-stack migration procedures can be interpreted through equation (1.53). Further analysis of it will explain the limitations of conventional processing procedures as well as suggest improvements in the procedures.

EXERCISES:

1 Adapt equation (1.48) to allow for a difference in velocity between the shot and the geophone.

2 Adapt equation (1.48) to allow for downgoing pressure waves and upcoming shear waves.

6.4 THE MEANING OF THE DSR EQUATION

The double-square-root equation contains most nonstatistical aspects of seismic data processing for petroleum prospecting. This equation, which was derived in the previous section, is not easy to understand because it is an operator in a four-dimensional space, namely, (z, s, g, t). We will approach it through various applications, each of which is like a picture in a space of lower dimension. In this section lateral velocity variation will be neglected (things are bad enough already!). Begin with

$$\frac{dU}{dz} = \frac{-\,i\omega}{v} \left(\sqrt{1 - G^2} + \sqrt{1 - S^2} \right) U \tag{6.54}$$

$$\frac{dU}{dz} = \frac{-\,i\omega}{v} \left(\sqrt{1 - (Y+H)^2} + \sqrt{1 - (Y-H)^2} \right) U \tag{6.55}$$

6.4.1 Zero-offset migration (H = 0)

One way to reduce the dimensionality of (1.55) is simply to set $H = 0$. Then the two square roots become the same, so that they can be combined to give the familiar paraxial equation:

$$\frac{dU}{dz} = -\,i\omega \frac{2}{v} \sqrt{1 - \frac{v^2\,k_y^2}{4\,\omega^2}}\; U \tag{6.56}$$

In both places in equation (1.56) where the rock velocity occurs, the rock velocity is divided by 2. Recall that the rock velocity needed to be halved in order for field data to correspond to the exploding-reflector model. So whatever we did by setting $H = 0$, gave us the same migration equation we used in chapter 3. Setting $H = 0$ had the effect of making the survey-sinking concept functionally equivalent to the exploding-reflector concept.

6.4.2 Zero-dip stacking (Y = 0)

When dealing with the offset h it is common to assume that the earth is horizontally layered so that experimental results will be independent of the midpoint y. With such an earth the Fourier transform of all data over y will vanish except for $k_y = 0$, or, in other words, for $Y = 0$. The two square roots in (1.54) and (1.55) again become identical, and the resulting equation is once more the paraxial equation:

$$\frac{dU}{dz} = -\,i\omega \frac{2}{v} \sqrt{1 - \frac{v^2\,k_h^2}{4\,\omega^2}}\; U \tag{6.57}$$

Using this equation to downward continue hyperboloids from the earth's surface, we find the hyperboloids shrinking with depth, until the correct depth where best focus occurs is reached. This is shown in Figure 1.28.

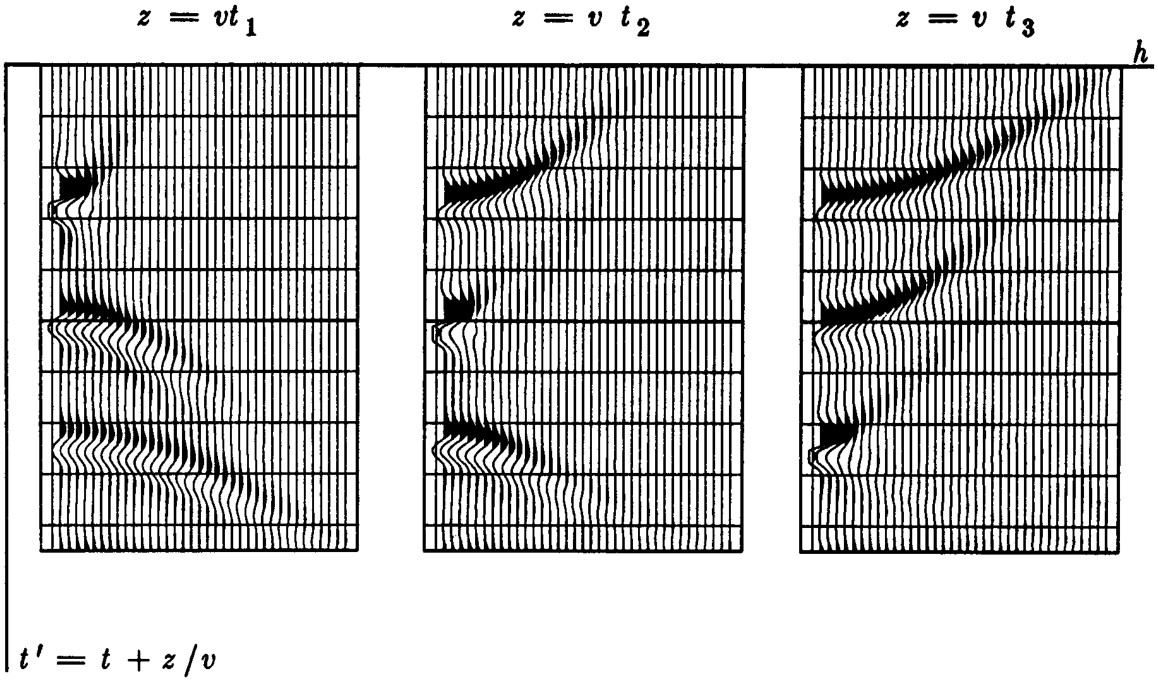

Figure 6.28: With an earth model of three layers, the common-midpoint gathers are three hyperboloids. Successive frames show downward continuation to successive depths where best focus occurs. ofs-dc2 [NR]

The waves focus best at zero offset. The focus represents a downward-continued experiment, in which the downward continuation has gone just to a reflector. The reflection is strongest at zero travel time for a coincident source-receiver pair just above the reflector. Extracting the zero-offset value at $t = 0$ and abandoning the other offsets is a way of eliminating noise. (Actually it is a way of *defining* noise). Roughly it amounts to the same thing as the conventional procedure of summation along a hyperbolic trajectory on the original data. Naturally the summation can be expected to be best when the velocity used for downward continuation comes closest to the velocity of the earth. Later, offset space will be used to *determine* velocity.

6.4.3 Conventional processing—separable approximation

The DSR operator is now defined as the parenthesized operator in equation (1b):

$$\mathrm{DSR}(Y, H) \quad = \quad \sqrt{1\ -\ (Y-H)^2}\ +\ \sqrt{1\ -\ (Y+H)^2} \tag{6.58}$$

In Fourier space, downward continuation is done with the operator $\exp(i\omega v^{-1}\,\mathrm{DSR}\,z)$.

There is a serious problem with this operator: it is *not separable* into a sum of an offset operator and a midpoint operator. *Nonseparable* means that a Taylor series for (1.58) contains terms like $Y^2 H^2$. Such terms cannot be expressed as a function of Y plus a function of H. Nonseparability is a data-processing disaster. It implies that migration and stacking must be done simultaneously, not sequentially. The only way to recover pure separability would be to return to the space of S and G. (That is a drastic alternative, far from conventional processing. We will return to it later).

Let us review the general issue of separability. The obvious way to get a separable approximation of the operator $\sqrt{1 - X^2 - Y^2}$ is to form a Taylor series expansion, and then drop all the cross terms. A more clever approximation is $\sqrt{1 - X^2} + \sqrt{1 - Y^2} - 1$, which fits all Y exactly when $X = 0$ and all X exactly when $Y = 0$. Applying this idea (though not the same equation) to the DSR operator gives

$$\mathrm{SEP}(Y,H) \;=\; 2 + [\mathrm{DSR}(Y,0) - 2] + [\mathrm{DSR}(0,H) - 2] \tag{6.59}$$

$$\mathrm{SEP}(Y,H) \;=\; 2\,[1 + (\sqrt{1 - Y^2} - 1) + (\sqrt{1 - H^2} - 1)] \tag{6.60}$$

Notice that at $H = 0$ (1.59) and (1.60) become equal to the DSR operator. At $Y = 0$ (1.59) and (1.60) also become equal to the DSR operator. Only when both H and Y are nonzero does SEP depart from DSR.

The splitting of (1.59) and (1.60) into a sum of three operators offers an advantage like the one offered by the 2-D Fourier kernel $\exp(ik_y y + ik_h h)$, which has a phase that is the sum of two parts. It means that Fourier integrals may have either y or h nested on the inside. So downward continuation with SEP could be done in (k_h, k_y)-space as implied by (1.55), or we could choose to Fourier transform to (h, k_y), (k_h, y), or (y, h) by appropriate nesting operations.

It is convenient to give familiar names to the three terms in (1.60). The first is associated with time-to-depth conversion, the second with migration, and the third with normal moveout.

$$\mathrm{SEP}(Y,H) \;=\; \mathrm{TD} + \mathrm{MIG}(Y) + \mathrm{NMO}(H) \tag{6.61}$$

The approximation (1.59) and (1.60) can be interpreted as "standard processing." The first stage in standard processing is NMO correction. In (1.59) and (1.60) the NMO operator downward continues all offsets at the earth's surface, to all offsets at depth. Selecting zero offset is no more than abandoning all other offsets. Like stacking over offset, selecting zero offset reduces the amount of data under consideration.

Ordinarily the abandoned offsets are not migrated. (Alternately, a clever procedure for changing stacking velocities after migration involves migrating several offsets near zero offset).

Since all terms in the SEP operator are interchangeable, it would seem wasteful to use it to migrate all offsets before stack. The result of doing so should be identical to after-stack migration.

6.4.4 Various meanings of H = 0

Recall the various forms of the stepout operator:

Forms of stepout operator $2H/v$		
ray trace	Fourier	PDE
$\frac{dt}{dh}$	$\frac{k_h}{\omega}$	$\partial_h^t \ = \ \int_{-\infty}^{t} dt \frac{\partial}{\partial h}$

Reciprocity suggests that travel time is a symmetrical function of offset; thus dt/dh vanishes at $h = 0$. In that sense it seems appropriate to apply equation (1.56) to zero-offset sections. More precisely, the ray-trace expression dt/dh strictly applies only when a single plane wave is present. Spherical wavefronts are made from the superposition of plane waves. Then the Fourier interpretation of H is slightly different and more appropriate. To set $\omega = 0$ would be to select a zero frequency component, a simple integral of a seismic trace. To set $k_h = 0$ would be to select a zero spatial-frequency component, that is, an integration over offset. Conventional stacking may be defined as integration (or summation) over offset along a hyperbolic trajectory. Simply setting $k_h = 0$ is selecting a hyperbolic trajectory that is flat, namely, the hyperbola of infinite velocity. Such an integration will receive its major contribution from the top of the data hyperboloid, where the data events come tangent to the horizontal line of integration. (For some historical reason, such a data summation is often called *vertical stack).* Of the total contribution to the integral, most comes from a zone near the top, before the stepout equals a half-wavelength. The width of this zone, which is called a Fresnel zone, is the major factor contributing to the integral. The Fresnel zone has been extracted from a field profile in Figure 1.29.

The definition of the Fresnel zone involves a frequency. For practical purposes we may just look at zero crossings. Examining Figure 1.29 near one second we see a variety of frequencies. In the interval between $t = 1.0$ and $t = 1.1$ I see about two wavelengths of low frequencies and about 5 wavelengths of high frequencies. The highest frequencies are the main concern, because they define the limit of seismic resolution. The higher frequency has about 100 half wavelengths between time zero and a time of one second. As a rough generality, this observed value of 100 applies to all travel times. That is, at any travel time, the highest frequency that has meaningful spatial correlations is often observed to have a half period of about 1/100 of the total travel time. We may say that the quality factor Q of the earth's sedimentary crust is often about 100. So the angle that we are typically thinking about is $\cos\ 8^\circ = \ .99$.

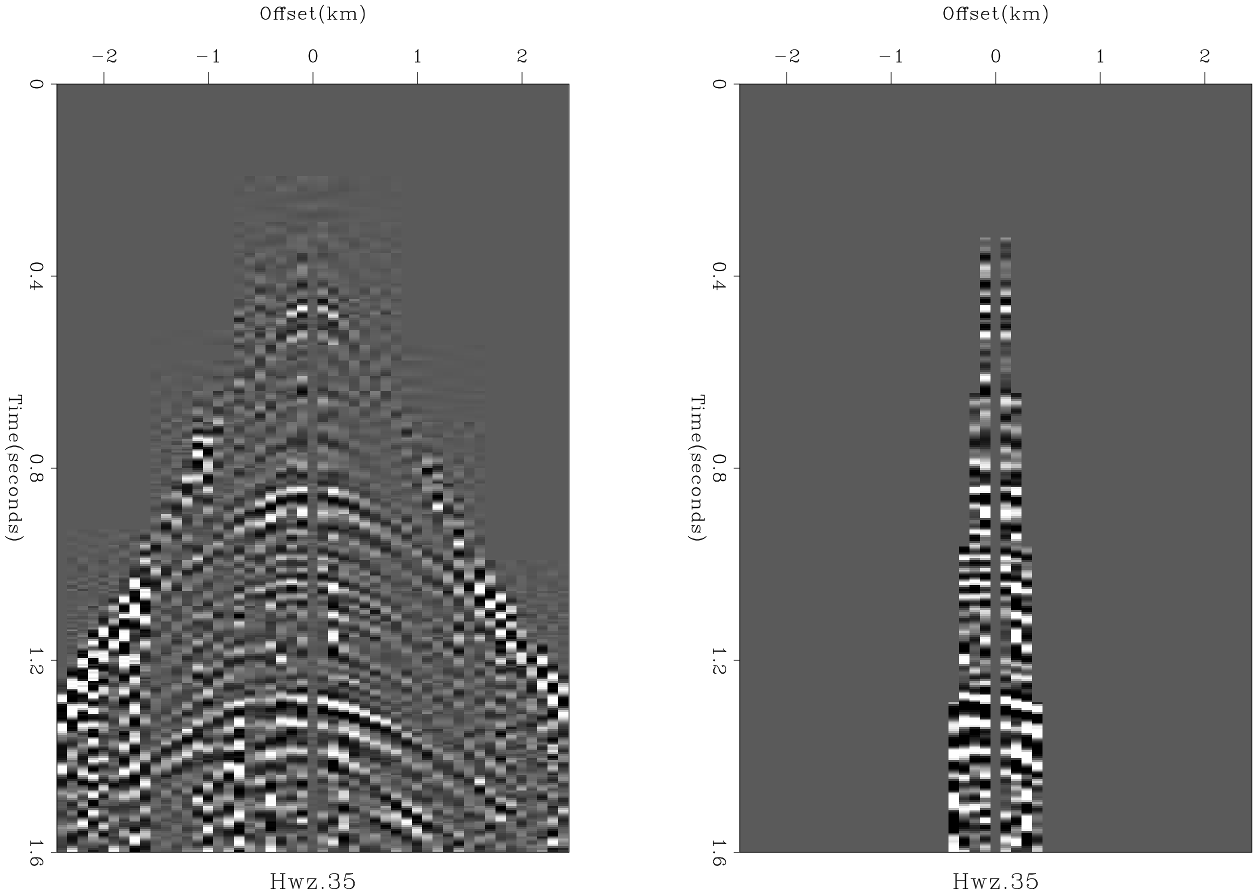

Figure 6.29: (left) A land profile from Denmark (Western Geophysical) with the Fresnel zone extracted and redisplayed (right). $\boxed{\text{ofs-denmark}}$ [ER]

Theoretically, the main differences between a zero-offset section and a vertical stack are the amplitude and a small phase shift. In practical cases they are unlikely to migrate in a significantly different way. It would be nice if we could find an equation to downward continue data that is stacked at velocities other than infinite velocity.

The partial-differential-equation point of view of setting $H = 0$ is identical with the Fourier view when the velocity is a constant function of the horizontal coordinate; but otherwise the PDE viewpoint is a slightly more general one. To be specific, but not cluttered, equations (1.54) and(1.55) can be expressed in 15° retarded, space-domain form. Thus,

$$\left[\frac{\partial}{\partial z} + \frac{v}{-\,i\omega\, 8} \left(\frac{\partial^2}{\partial y^2} + \frac{\partial^2}{\partial h^2} \right) \right] U' \quad = \quad 0 \tag{6.62}$$

Integrate this equation over offset h. The integral commutes with the differential operators. Recall that the integral of a derivative is the difference between the function evaluated at the upper limit and the function evaluated at the lower limit. Thus,

$$\left(\frac{\partial}{\partial z} + \frac{v}{-\,i\omega\, 8} \frac{\partial^2}{\partial y}^2 \right) \left(\int U\, dh \right) + \frac{v}{-\,i\omega\, 8} \frac{\partial U}{\partial h} \Bigg|_{h\ =\ -\infty}^{h\ =\ +\infty} = 0 \tag{6.63}$$

The wave should vanish at infinite offset and so should its horizontal offset derivative. Thus the last term in (1.63) should vanish. So, setting $H = 0$ has the meaning

$$\text{(Paraxial operator} \quad \text{(vertical stack} \quad = \quad 0 \tag{6.64}$$

A problem in the development of (1.64) was that, twice, it was assumed that velocity is independent of offset: first, when the thin-lens term was omitted from (1.62), and second, when the offset integration operator was interchanged with multiplication by velocity. If the velocity depends on the horizontal x-axis, then it certainly depends on both midpoint and offset. In conclusion: If velocity changes slowly across a Fresnel zone, then setting $H = 0$ provides a valid equation for downward continuation of vertically stacked data.

6.4.5 Clayton's cosine corrections

A tendency exists to associate the sine of the earth dip angle with Y and the sine of the shot-geophone offset angle with H. While this is roughly valid, there is an important correction. Consider the dipping bed shown in Figure 1.30.

The dip angle of the reflector is α, and the offset is expressed as the offset angle β. Clayton showed, and it will be verified, that

$$Y \quad = \quad \sin\,\alpha \quad \cos\,\beta \tag{6.65}$$

$$H \quad = \quad \sin\,\beta \quad \cos\,\alpha \tag{6.66}$$

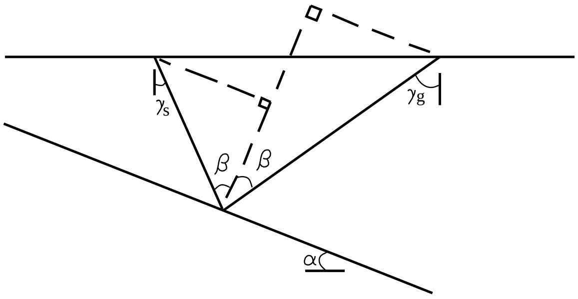

Figure 6.30: Geometry of a dipping bed. The line bisecting the angle 2β does not pass through the midpoint between g and s. (Clayton) ofs-clay [NR]

For small positive or negative angles the cosines can be ignored, and it is then correct to associate the sine of the earth dip angle with Y and the sine of the offset angle with H. At moderate angles the cosine correction is required. At angles exceeding 45° the sensitivities reverse, and conventional wisdom is exactly opposite to the truth. The reader should be wary of informal discussions that simply associate Y with dip and H with velocity. "Larner's streaks" were an example of mixing the effects of dip and offset. Indeed, at steep dips the usual procedure of using H to determine velocity should be changed somehow to use Y.

Next, (1.65) and (1.66) will be proven. The source takeoff angle is γ_s, and the incident receiver angle is γ_g. First, relate γ_s and γ_g to α and β. Adding up the angles of the smaller constructed triangle gives

$$\left(\frac{\pi}{2} - \gamma_s - \alpha\right) + \beta + \frac{\pi}{2} = \pi$$
$$\gamma_s = \beta - \alpha \tag{6.67}$$

Adding up the angles around the larger triangle gives

$$\gamma_g = \beta + \alpha \tag{6.68}$$

To associate the angles at depth, α and β, with the stepouts dt/ds and dt/dg at the earth's surface requires taking care with the signs, noting that travel time increases as the geophone moves right and decreases as the shot moves right. Recall from equations (1.46), (1.47), (1.49), (1.50), (1.51) and (1.52), the definitions of apparent angles Y and H,

$$Y - H = S = \frac{v\,k_s}{\omega} = v\,\frac{dt}{ds} = -\sin\gamma_s = \sin(\alpha - \beta) \tag{6.69}$$
$$Y + H = G = \frac{v\,k_g}{\omega} = v\,\frac{dt}{dg} = +\sin\gamma_g = \sin(\alpha + \beta) \tag{6.70}$$

Adding and subtracting this pair of equations and using the angle sum formula from trigonometry gives Clayton's cosine corrections (8):

$$Y = \frac{1}{2}\sin(\alpha + \beta) + \frac{1}{2}\sin(\alpha - \beta) = \sin\alpha\,\cos\beta \tag{6.71}$$
$$H = \frac{1}{2}\sin(\alpha + \beta) - \frac{1}{2}\sin(\alpha - \beta) = \sin\beta\,\cos\alpha \tag{6.72}$$

6.4.6 Snell-wave stacks and CMP slant stacks

Setting the takeoff angle S to zero also reduces the double-square-root equation to a single-square-root equation. The meaning of $S = 0$ is that $k_s = 0$ or equivalently that the data should undergo a summation (without time shifting) over shot s. Such a summation simulates a downgoing plane wave. The imaging principle behind the summation would be to look at the upcoming wave at the arrival time of the downgoing wave. S could also be set equal a constant, to simulate a downgoing Snell wave.

A Snell wave is a generalization of a downgoing plane wave at nonvertical incidence. The shots are not fired simultaneously, but sequentially at an inverse rate of $dt/ds = S/v$. This could be simulated with field data by summing across the (t, s)-plane along a line of slope dt/ds. Setting S to be some constant, say $S = v\ dt/ds$, also reduces the double-square-root equation to a paraxial wave equation, just the equation needed to downward continue the downgoing Snell wave experiment. Snell waves could be constructed for various $p = dt/ds$ values. Each could be migrated and imaged, and the images stacked over p. These ideas have been around longer than the DSR equation, yet they have gained no popularity. What could be the reason?

A problem with Snell wave simulation is that the wavefield is usually sampled at coarse intervals along a geophone cable, which itself never seems to extend as far as the waves propagate. Crafty techniques to interpolate and extrapolate the data are frustrated by the fact that on a common-geophone gather, the top of the hyperbola need not be at zero offset. For dipping beds the earliest arrival is often off the end of the cable. So the data processing depends strongly on the missing data.

These difficulties provide an ecological niche for the common-midpoint slant stack, namely, $H = pv$. (A fuller explanation of slant stack comes later.) At common *midpoint* the hyperbolas go through zero offset with zero slope. The data are thus more amenable to the interpolation and extrapolation required for integration over a slanted line. Setting $H = pv$ yields

$$k_z \quad = \quad -\frac{\omega}{v} \left[\sqrt{1 - (Y + pv)^2} + \sqrt{1 - (Y - pv)^2} \right] \tag{6.73}$$

This has not reduced the DSR equation to a paraxial wave equation, but it has reduced the problem to a form manageable with the available techniques, such as the Stolt or phase-shift methods. Details of this approach can be found in the dissertation of Richard Ottolini [1982].

6.4.7 Why not downward continue in (S,G)-space?

If the velocity were known and the only task were to migrate, then there would be no fundamental reason why the downward continuation could not be done in (S, G)-space. But the velocity really isn't well known. The sensitivity of migration to velocity error increases rapidly with angle, and angle accuracy is the presumed advantage of (S, G)-space. Furthermore, the finite extent of the recording cable and the tendency to spatial aliasing create the same problems with (S, G)-space migration as are experienced with Snell stacks. I see no fundamental reason why (S, G)-space migration should be any better than CMP slant stacks, and the aliasing and truncation situations seem likely to be worse. Less ambitious and more practical approaches to the wide-angle migration problem are found later in this chapter.

On the other hand, lateral velocity variation (if known) could demand that migration be done in (s, g)-space.

Still another reason to enter shot-geophone space would be that the shots were far from one another. Then the data would be aliased in both midpoint space and offset space.

Index